

## The Higgs Mass beyond the CMSSM

John Ellis<sup>1,2</sup>, Feng Luo<sup>1</sup>, Keith A. Olive<sup>3</sup> and Pearl Sandick<sup>4</sup>

<sup>1</sup>*Theoretical Physics and Cosmology Group, Department of Physics, King's College London,  
London WC2R 2LS, UK*

<sup>2</sup>*TH Division, Physics Department, CERN, CH-1211 Geneva 23, Switzerland*

<sup>3</sup>*William I. Fine Theoretical Physics Institute, School of Physics and Astronomy,  
University of Minnesota, Minneapolis, MN 55455, USA*

<sup>4</sup>*Department of Physics, University of Utah, Salt Lake City, Utah 84112, USA*

### Abstract

The apparent discovery of a Higgs boson with mass  $\sim 125$  GeV has had a significant impact on the constrained minimal supersymmetric extension of the Standard Model in which the scalar masses, gaugino masses and tri-linear  $A$ -terms are assumed to be universal at the GUT scale (the CMSSM). Much of the low-mass parameter space in the CMSSM has been excluded by supersymmetric particle searches at the LHC as well as by the Higgs mass measurement and the emergent signal for  $B_s \rightarrow \mu^+ \mu^-$ . Here, we consider the impact of these recent LHC results on several variants of the CMSSM with a primary focus on obtaining a Higgs mass of  $\sim 125$  GeV. In particular, we consider the one- and two-parameter extensions of the CMSSM with one or both of the Higgs masses set independently of the common sfermion mass,  $m_0$  (the NUHM1,2). We also consider the one-parameter extension of the CMSSM in which the input universality scale  $M_{in}$  is below the GUT scale (the sub-GUT CMSSM). We find that when  $M_{in} < M_{GUT}$  large regions of parameter space open up where the relic density of neutralinos can successfully account for dark matter with a Higgs boson mass  $\sim 125$  GeV. In some of these regions essential roles are played by coannihilation processes that are usually less important in the CMSSM with  $M_{in} = M_{GUT}$ . Finally, we reconsider mSUGRA models with sub-GUT universality, which have the same number of parameters as the CMSSM. Here too, we find phenomenologically viable regions of parameter space, which are essentially non-existent in GUT-scale mSUGRA models. Interestingly, we find that the preferred range of the  $A$ -term straddles that predicted by the simplest Polonyi model.

# 1 Introduction

Supersymmetry is one of the best-motivated extensions of the Standard Model, including the naturalness of the electroweak scale, the appearance of a candidate for the cold dark matter if  $R$ -parity is conserved, unification of the fundamental interactions, the prediction of a Higgs boson weighing  $\lesssim 130$  GeV, and the stabilization of the electroweak vacuum if the Higgs boson weighs  $\lesssim 127$  GeV, as seems now to be the case. For these and other, more theoretical reasons, much attention has been focused on models with supersymmetric particles weighing  $\lesssim 1$  TeV, and notably the simplest, minimal supersymmetric extension of the Standard Model (the MSSM). In particular, many studies have been made of the simplified variant in which the soft supersymmetry-breaking scalar masses, gaugino masses and tri-linear  $A$ -terms are assumed to originate at some high mass scale and be universal at the supersymmetric GUT scale (the CMSSM) [1–5].

However, there is as yet no direct evidence for supersymmetry. Some years ago, hopes were high that the deviation of the experimental measurement of the anomalous magnetic moment of the muon,  $g_\mu - 2$  [6], from the prediction of the Standard Model might herald the appearance of low-mass supersymmetric particles accessible to the initial run of the LHC. However, this has not yet transpired, and the continuing absence of supersymmetric particles at the LHC [7] is putting increasing pressure on the CMSSM and rendering the supersymmetric interpretation of  $g_\mu - 2$  somewhat dubious in this and related models.

The ATLAS and CMS experiments have recently discovered a new boson with spin  $\neq 1$  and couplings similar to those of the Standard Model Higgs boson [8]. This is compatible with such simple supersymmetric models, which predict not only the existence of a Higgs boson with mass  $\lesssim 130$  GeV, but also that its couplings to Standard Model particles should be indistinguishable from those in the Standard Model at the present level of accuracy. Using `FeynHiggs` [9] there is an uncertainty  $\sim \pm 1.5$  GeV in the prediction for the Higgs mass for any given set of input CMSSM parameters, but the measurement of a mass  $\sim 125$  to 126 GeV does disfavour relatively low sparticle masses. Taken together with the absence so far of supersymmetric particles at the LHC, the Higgs mass measurement excludes a large range of low-mass CMSSM parameters [10–14].

In parallel, increasing pressure is being placed on models with large  $\tan \beta$  by the strengthening experimental constraint on the decay  $B_s \rightarrow \mu^+ \mu^-$  [15], in particular the recent detection by LHCb of  $B_s \rightarrow \mu^+ \mu^-$  with a value close to the Standard Model prediction [16]. Currently, the 95% upper limit on the branching fraction relative to the Standard Model value is 1.65 from LHCb alone, improving to 1.50 when combined with other experiments.

These developments motivate the study of generalizations of the CMSSM, the search for viable alternatives, and the exploration of their observational signatures, with a view to future searches at the LHC and elsewhere.

In this spirit, here we consider various one- and two-parameter extensions of the CMSSM. One option that has often been studied is to allow one or both of the soft supersymmetry-breaking contributions to Higgs scalar masses to be independent of the common sfermion mass,  $m_0$  (the NUHM1,2) [17–20]. These offer some extra possibilities for accommodating the mass of the Higgs boson and the absence (so far) of supersymmetric particles at the LHC

while yielding the appropriate relic cold dark matter density.

Another way to extend the CMSSM with one additional parameter is to allow the input universality scale to be lower than the GUT scale [21] (the sub-GUT CMSSM). In this case, the sparticle spectrum is compressed relative to that in the CMSSM, because of the reduced amount of renormalization of the soft supersymmetry-breaking masses if they are universal below the GUT scale. This in turn implies that relatively large ranges of sparticle masses are compatible simultaneously with a Higgs boson mass  $\sim 125$  GeV and an appropriate relic dark matter density, often involving novel coannihilation mechanisms not relevant in the CMSSM.

As a corollary, one may impose an additional constraint on the sub-GUT extension of the CMSSM and retain many of its phenomenological advantages. In particular, one may impose the specific relation  $A_0 = B_0 + m_0$  between the trilinear and bilinear soft supersymmetry-breaking parameters  $A_0$  and  $B_0$  that is characteristic of minimal supergravity (mSUGRA) theories [22–24]. Intriguingly, we find acceptable models for a range of  $A_0$  values that includes the specific value  $A_0 = (3 - \sqrt{3}) \times m_{3/2}$  found in the original Polonyi model [25].

A generic feature of the NUHM1,2 and such sub-GUT models is the increased importance of coannihilation effects, that are only important along narrow strips in the CMSSM parameter space. Accordingly, in this paper we have paid particular attention to the treatment of coannihilation processes, using a more complete treatment than in our previous analyses of the NUHM1,2 [18, 20] and sub-GUT models [21].

The layout of this paper is as follows. In Section 2 we recall relevant features of gravity-mediated models such as mSUGRA and the CMSSM, as well as pointing out some important features of their extensions to the NUHM and sub-GUT models. In Section 3, we discuss in more detail the impact of the LHC constraints and briefly review the current constraints on the CMSSM and mSUGRA. Section 4 discusses the impact of the LHC constraints on the NUHM1,2, Section 5 discusses sub-GUT generalizations of the CMSSM, and Section 6 discusses the specific case of sub-GUT mSUGRA. Finally, Section 7 summarizes our principal conclusions.

## 2 mSUGRA, the CMSSM and Generalizations

### 2.1 mSUGRA

We start by recalling relevant aspects of minimal supergravity (mSUGRA) models, which have a flat Kähler potential and a low-energy scalar potential that can be written as [22–24]

$$V = \left| \frac{\partial W}{\partial \phi^i} \right|^2 + (A_0 W^{(3)} + B_0 W^{(2)} + h.c.) + m_{3/2}^2 \phi^i \phi_i^*, \quad (1)$$

where  $W$  is the superpotential for matter fields,

$$W = (y_e H_1 L e^c + y_d H_1 Q d^c + y_u H_2 Q u^c) + \mu H_1 H_2, \quad (2)$$

and the SU(2) indices have been suppressed. In (1),  $W^{(3)}$  is the trilinear part of the superpotential,  $W^{(2)}$  is the bilinear part, and  $m_{3/2}$  is the gravitino mass. This is the order

parameter for local supersymmetry breaking, and in mSUGRA one finds scalar mass universality,  $m_0 = m_{3/2}$ . This condition is applicable at some input renormalization scale,  $M_{in}$ , which is usually associated with the grand unification scale. In addition, in mSUGRA there is a relation between the tri- and bilinear supersymmetry breaking terms,  $A_0 = B_0 + m_0$ . With a minimal choice for the gauge kinetic function, gaugino mass universality characterized by  $m_{1/2}$  is also obtained, which is usually imposed at the same input scale  $M_{in}$ .

Minimization of the Higgs potential leads to two vacuum conditions at the weak scale, which can be expressed as

$$\mu^2 = \frac{m_1^2 - m_2^2 \tan^2 \beta + \frac{1}{2} m_Z^2 (1 - \tan^2 \beta) + \Delta_\mu^{(1)}}{\tan^2 \beta - 1 + \Delta_\mu^{(2)}}, \quad (3)$$

and

$$B\mu = -\frac{1}{2}(m_1^2 + m_2^2 + 2\mu^2) \sin 2\beta + \Delta_B, \quad (4)$$

where  $m_{1,2}$  are the soft supersymmetry-breaking Higgs masses (evaluated at the weak scale),  $\tan \beta$  is the ratio of the two Higgs vacuum expectation values, and  $\Delta_B$  and  $\Delta_\mu^{(1,2)}$  are loop corrections [26]. As a result, an mSUGRA model can be defined in terms of just 3 continuous parameters:  $m_{1/2}$ ,  $m_0$  and  $A_0$ , and the sign of  $\mu$ . Together, these determine  $\tan \beta$  and the magnitude of  $\mu$  via the vacuum conditions (3, 4).

## 2.2 The CMSSM

The CMSSM is the most thoroughly studied of all classes of constrained supersymmetric models [1–5]. It is a two-parameter generalization of mSUGRA, in which the relation between  $A_0$  and  $B_0$  is dropped, allowing one to treat  $\tan \beta$  as a free parameter, as well as dropping the relationship between the universal sfermion mass  $m_0$  and the gravitino mass, which is possible if the supergravity Kähler potential includes non-minimal kinetic terms. Thus, the CMSSM is defined by the sign of  $\mu$ ,  $m_{1/2}$ ,  $m_0$ ,  $A_0$ ,  $\tan \beta$ , and  $m_{3/2}$ , though the latter is usually ignored, e.g., because it is assumed implicitly to be irrelevantly large. We note that the CMSSM can be directly related to mSUGRA [27] through an extension in which terms proportional to  $W^{(2)}$  are added to the Kähler potential as in the Giudice-Masiero mechanism [28]. For example, a contribution to  $K$  of the form

$$\Delta K = c_H H_1 H_2 + h.c., \quad (5)$$

where  $c_H$  is a constant, and  $H_{1,2}$  are the usual MSSM Higgs doublets, affects the boundary conditions for both  $\mu$  and the  $B$  term at the supersymmetry breaking input scale,  $M_{in}$ , in a manner similar to the CMSSM.

## 2.3 The NUHM1,2

One of the possible one-parameter extensions of the CMSSM is the oft-studied NUHM1 [17, 18], in which the soft supersymmetry-breaking Higgs masses are taken to be equal to each

other, but are allowed to differ from the otherwise universal sfermion mass,  $m_1 = m_2 \neq m_0$ . We also discuss here a two-parameter extension of the CMSSM, namely the NUHM2 [20] in which  $m_1 \neq m_2 \neq m_0$ , in general.

## 2.4 Sub-GUT versions of CMSSM and mSUGRA

Another one-parameter generalization of the CMSSM is provided by models in which the input scale for supersymmetry breaking universality differs from the GUT scale. Although  $M_{in}$  might be chosen above the GUT scale [27, 29, 30], such a choice would introduce many more parameters associated with different GUT models, and its study lies beyond the scope of this work. Here we concentrate on ‘sub-GUT’ models in which  $M_{in} < M_{GUT}$  [21], which can be related to mirage unification models [31].

Both the NUHM1 and sub-GUT CMSSM are six-parameter models (five if one neglects the gravitino mass, e.g., by assuming that it is irrelevantly large). As we shall see, both the NUHM1,2 and sub-GUT models allow a suitable relic dark matter density and a Higgs mass of 125 GeV to be achieved simultaneously. This is also the case in sub-GUT versions of mSUGRA. This is a four-parameter class of models ( $m_{1/2}, m_{3/2}, A_0$ , and  $M_{in}$ ). Interestingly, we find that such models are phenomenologically viable in a relatively restricted range for  $A_0$ , which straddles the Polonyi value  $A_0 = (3 - \sqrt{3}) \times m_{3/2}$  [24, 25].

As an appetizer for the subsequent discussion, we display in the left panel of Fig. 1 the evolution of the sparticle spectrum with  $M_{in} < M_{GUT}$  for a typical Polonyi mSUGRA scenario with  $m_{1/2} = m_0 = 2000$  GeV. At these values of  $(m_{1/2}, m_0)$ ,  $\tan \beta$  varies from  $\sim 18$  when  $M_{in} = M_{GUT}$  to  $\sim 43$  when  $M_{in} = 3 \times 10^8$  GeV: we do not find consistent electroweak vacuum solutions much below this value of  $M_{in}$ , as indicated by the mauve shading in Fig. 1. As  $M_{in}$  decreases, we see that the spectrum compresses until  $M_{in} \sim 10^{10.5}$  GeV with, in particular, the approach of  $m_{\chi_3}$  and  $m_{\chi_2}$  to  $m_\chi$ . This has the general effect of enhancing the importance of coannihilation processes that are less suppressed by Boltzmann factors  $\sim \exp(-\Delta m/T)$ . We also note that  $m_\chi \simeq m_A/2$  when  $M_{in} \sim 10^{12}$  GeV, indicating that the parameters traverse a rapid s-channel annihilation funnel region. There is level crossing in the neutralino spectrum when  $M_{in} \sim 10^{10.5}$  GeV, with the composition of the lightest supersymmetric particle (LSP)  $\chi$  making a transition from almost pure bino to almost pure Higgsino, as seen in the right panel of Fig. 1. For  $M_{in} \lesssim 10^{10.5}$  GeV, the LSP and the next-to-lightest supersymmetric particle (NLSP) are nearly degenerate Higgsinos, with important implications for annihilation rates. We also note that their masses approach  $m_A/2$  again just below  $10^9$  GeV, so that rapid (co)annihilations via s-channel  $H/A$  poles again become important.

This example illustrates just some of the variety of (co)annihilation phenomena that can control the relic LSP density in sub-GUT models. More of the possible richness will be seen in subsequent figures.

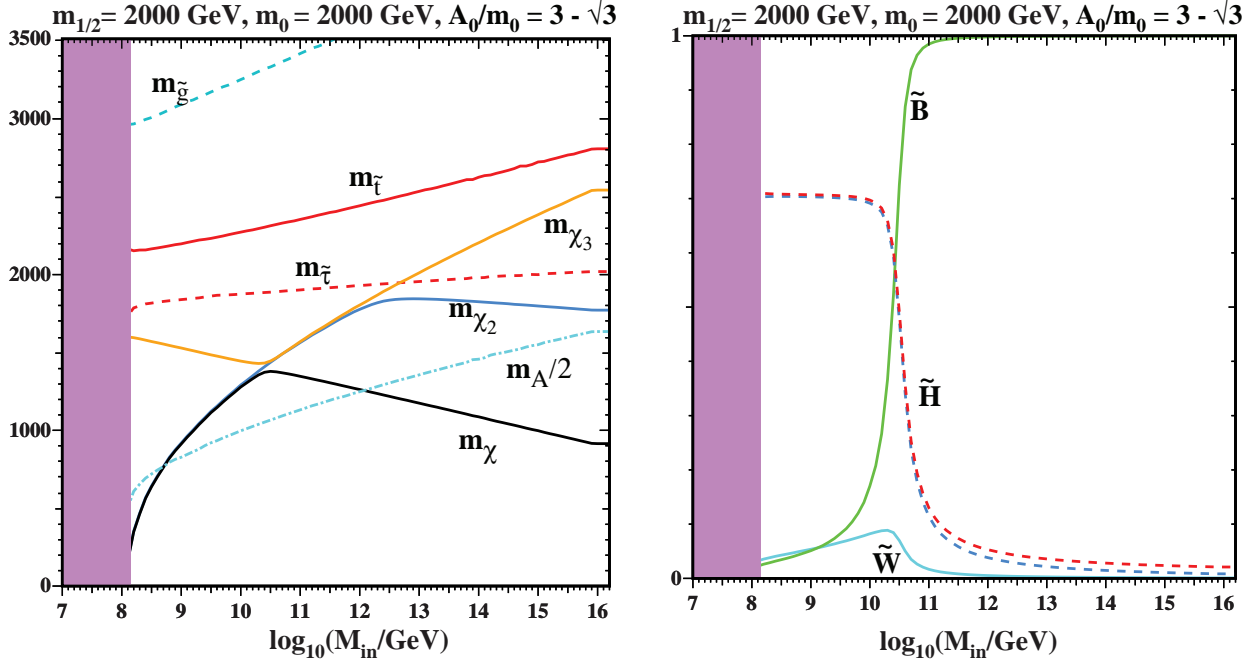


Figure 1: *The evolution of (left) the sparticle spectrum and (right) the composition of the LSP  $\chi$  as functions of  $M_{in}$  in a specific sub-GUT Polonyi  $mSUGRA$  scenario with  $m_{1/2} = m_0 = 2000$  GeV.*

### 3 The Impacts of Recent LHC Results on the CMSSM and $mSUGRA$

The following are the principal experimental, phenomenological and cosmological constraints on supersymmetric models that we consider in this paper:

- The preferred cosmological cold dark matter density range is [32]:  $\Omega_{CDM}h^2 = 0.112 \pm 0.006$ , where  $h$  is the present Hubble expansion rate in units of 100 km/s/Mpc. We emphasize models in which the lightest supersymmetric particle (LSP), assumed here to be the lightest neutralino,  $\chi$ , is the dominant source of cold dark matter [33]. In general, supersymmetric models in which the LSP density is not excessive are squeezed closer to the boundaries where the LSP becomes charged or there is no consistent solution to the electroweak vacuum conditions (3, 4), and do not have very different values of the input parameters.
- The strongest upper limit on the spin-independent cold dark matter scattering cross section is from XENON100 [34], which excludes the focus-point region of the CMSSM and some analogous regions in models with more parameters [10].
- The anomalous magnetic moment of the muon,  $g_\mu - 2$ , will be treated as an optional constraint [6], unlike the previous constraints, which are considered to be mandatory.

- Constraints are provided by flavour physics, in particular by  $b \rightarrow s\gamma$  [35] and  $B_s \rightarrow \mu^+\mu^-$  [15,16], the latter now being dominated by the measurement by LHCb and upper limits from the other LHC experiments.
- ATLAS and CMS provide limits from searches for missing-energy events at the LHC, in particular the ATLAS search with  $\sim 5/\text{fb}$  of data at 8 TeV [7,36], which is currently the most sensitive public result.
- The measured mass of the (lightest) Higgs boson is taken as  $M_h = 125.7 \pm 1.0$  GeV [8]. We recall that the theoretical calculation uncertainty of  $M_h$  for any given set of input parameters for the CMSSM or a similar model is typically  $\sim 1.5$  GeV, so any parameter set yielding  $M_h \geq 124$  GeV could probably be regarded as acceptable.

### 3.1 Impacts on CMSSM models

Fig. 2 displays the interplays of these constraints in the  $(m_{1/2}, m_0)$  planes of the CMSSM for four choices of the input parameters  $A_0$  and  $\tan\beta$ , assuming in all cases that  $\mu > 0$ <sup>1</sup>. The left panels of Fig. 2 are for  $\tan\beta = 10$ , and the right panels are for  $\tan\beta = 40$ . The upper panels are for  $A_0 = 0$ , and the lower panels are for  $A_0 = 2.5m_0$ . In each panel, the region at high  $m_{1/2}$  and low  $m_0$  where the  $\tilde{\tau}_1$  is the LSP is shaded brown, and the region at low  $m_{1/2}$  and high  $m_0$  where there is no consistent solution to the vacuum conditions (3, 4) is shaded mauve. The regions excluded by  $b \rightarrow s\gamma$  are shaded green, those favoured by  $g_\mu - 2$  are shaded pink, and those favoured by  $\Omega_\chi h^2$  are shaded dark blue<sup>2</sup>. The LEP chargino exclusion is shown as a near-vertical dashed black line at small  $m_{1/2}$  [37].

Turning to the LHC constraints, contours of  $M_h$  are shown in all panels as red dash-dotted lines, and the ATLAS exclusion from the search for events with missing transverse energy (MET) is shown as a solid purple line<sup>3</sup>. We also display as solid green lines three contours of  $\text{BR}(B_s \rightarrow \mu^+\mu^-)/\text{BR}(B_s \rightarrow \mu^+\mu^-)_{SM} = 1.65, 1.5$  (the present 95% CL upper limit from LHCb and combined experiments), 1.3 (the 68% upper limit from LHCb). For reference, where relevant we also show the contours for 1.0 (the Standard Model value) and 0.85 (corresponding to the central value seen at LHCb). The same shadings and line styles are used in all subsequent figures.

Concerning the impacts of the LHC constraints, we see in the upper panels that  $M_h$  is in general too small if  $A_0 = 0$ . We also see that the MET constraint allows only the upper

<sup>1</sup>Historically, this sign of  $\mu$  has been favoured by the supersymmetric interpretation of  $g_\mu - 2$  (we display  $g_\mu - 2$ -compatible regions in Fig. 2 but not in subsequent figures) and to facilitate compatibility with  $b \rightarrow s\gamma$ . However, since the LHC constraints now disfavour regions of the CMSSM parameter space that ‘explain’ the  $g_\mu - 2$  discrepancy (as seen in Fig. 2), this assumption should be taken with a grain of salt.

<sup>2</sup>Because of the combination of recent experimental constraints, we are forced to consider substantially larger ranges in the displayed supersymmetric parameters such as  $m_0$  and  $m_{1/2}$ . Therefore, here and in many other figures, for reasons of visibility we shade wider strips where  $0.06 < \Omega_\chi h^2 < 0.2$ .

<sup>3</sup>As discussed in [10], this limit is generally stronger than other direct searches for supersymmetry at the LHC in the models studied, and is largely independent of  $\tan\beta$  and  $A_0$ . Based on the analysis in [39], in the upper left panel of Fig. 2 we have assumed that the constraint published in [36] is independent of  $m_{1/2}$  when extrapolated to lower  $m_0$ .

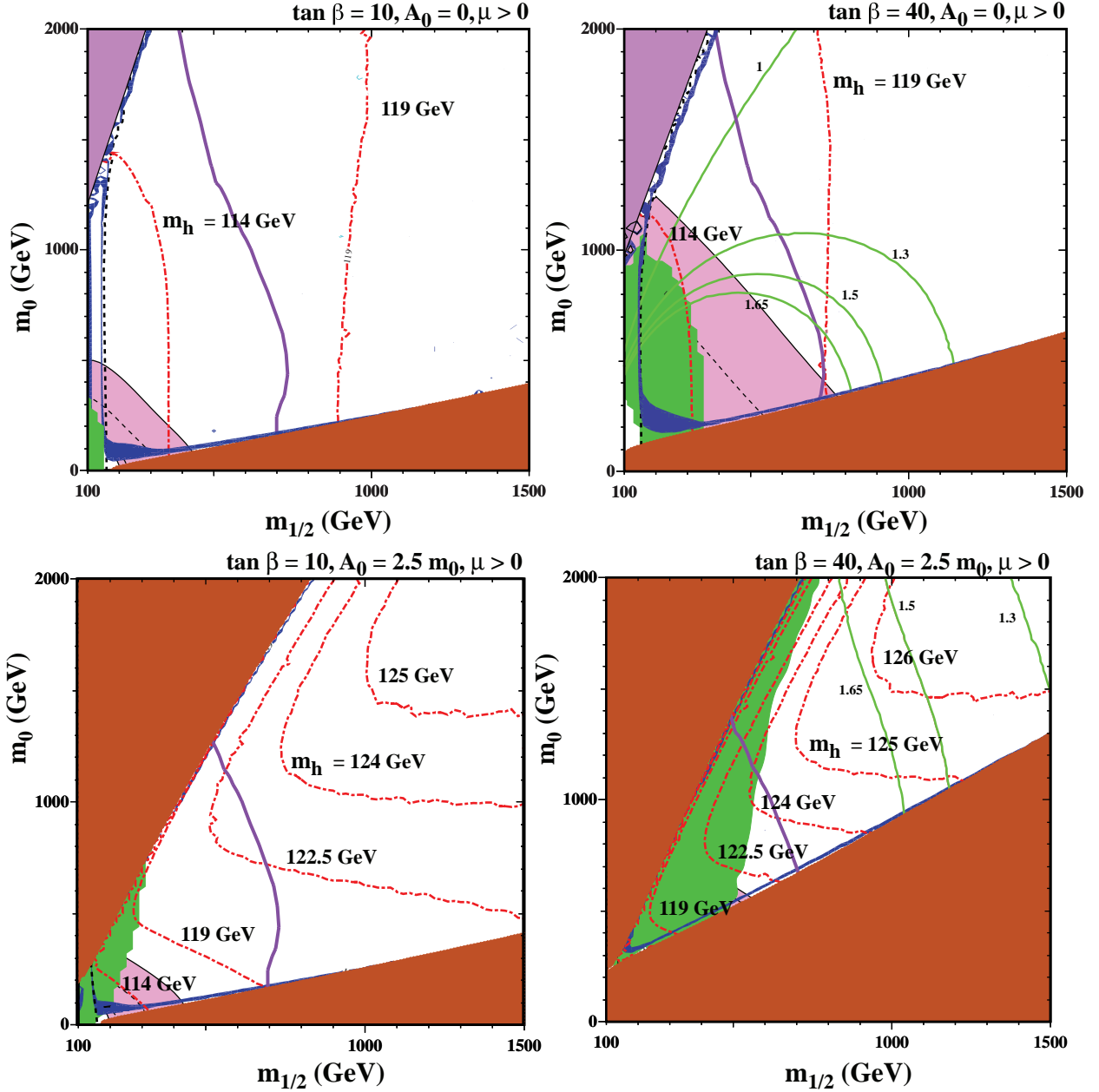


Figure 2: The CMSSM  $(m_{1/2}, m_0)$  planes for  $\mu > 0$ , with  $\tan \beta = 10$  (left) and 40 (right),  $A_0 = 0$  (upper) and  $A_0 = 2.5 m_0$  (lower), as calculated for  $m_t = 173.2$  GeV using the latest version of the SSARD code [38]. The interpretations of the shadings and contour colours are described in the text.

end of the coannihilation strip close to the  $\tilde{\tau}_1$  LSP boundary<sup>4</sup>, and is incompatible with a supersymmetric resolution of the  $g_\mu - 2$  discrepancy. The  $B_s \rightarrow \mu^+ \mu^-$  constraint has no

<sup>4</sup>We recall that the focus-point strip is excluded by the XENON100 upper limit on spin-independent dark matter scattering.



impact for  $\tan\beta = 10$ , but for  $\tan\beta = 40$ ,  $A_0 = 0$  its restriction on the coannihilation strip is stronger than that of the MET constraint.

In the lower panels, we see that  $M_h$  is generally larger when  $A_0 = 2.5 m_0$ . However, for  $\tan\beta = 10$ ,  $M_h$  does not grow above  $\sim 121$  GeV, whereas for  $\tan\beta = 40$ ,  $A_0 = 2.5 m_0$  there is compatibility for  $m_{1/2} \gtrsim 1$  TeV along the coannihilation strip. This region is also compatible with the LHC MET constraint, but not with the supersymmetric interpretation of  $g_\mu - 2$ . Note that for the larger values of  $A_0$ , we see another brown shaded region in the upper left where the stop becomes the LSP (or tachyonic). To the right of this boundary there is a stop coannihilation strip which occurs at relatively low  $M_h$  when  $\tan\beta = 10$  and is in the region excluded by  $b \rightarrow s\gamma$  when  $\tan\beta = 40$ . Once again, the  $B_s \rightarrow \mu^+\mu^-$  constraint has no impact for  $\tan\beta = 10$ , and requires large  $m_{1/2}$  for  $\tan\beta = 40$ . The disconnect between the LHC results and the potential solution to the  $g_\mu - 2$  discrepancy is severe enough that we will not show the  $g_\mu - 2$  compatible regions in future plots.

A more complete survey of CMSSM models with other values of  $A_0$  is given in [14], but this brief summary serves to illustrate how the LHC constraints prefer larger values of  $\tan\beta$ ,  $A_0$  and  $m_{1/2}$ .

### 3.2 Impacts on mSUGRA models

In Fig. 3 we show a pair of mSUGRA  $(m_{1/2}, m_0)$  planes for  $\mu > 0$ . We recall that, there is just one free parameter in addition to these, which may be taken as  $A_0$ : the electroweak vacuum conditions (3, 4) may be used to determine  $\tan\beta$  at each point on the plane [40]. In the left panel, we adopt the value  $A_0 = (3 - \sqrt{3}) m_0$  found in the original Polonyi model. Contours of fixed  $\tan\beta$  are shown by the grey solid curves in increments of 5, as labelled. Also shown, as a diagonal and solid light blue line, is the contour where  $m_{3/2} = \min(m_\chi, m_{\tilde{\tau}_1})$ , below which the gravitino is the LSP. Another diagonal line (brown dotted) shows the contour where the lightest neutralino mass  $m_\chi$  is equal to the mass of the lighter stau,  $m_{\tilde{\tau}_1}$ . The latter appears below the gravitino LSP line, so the  $\tilde{\tau}_1$  is never the LSP in this particular model. As a consequence, only the dark blue shaded region at low  $m_{1/2}$  above the light blue line corresponds to neutralino dark matter with the WMAP density. The dark blue shaded region below the light blue line corresponds to the gravitino LSP having the WMAP density it would have if there is no non-thermal contribution to the gravitino density. Here, the gravitino density is determined from the (co)annihilations of the NLSP - either the neutralino or (if below the dotted line) the lighter stau - followed by decay of the NLSP into the gravitino LSP, resulting in  $\Omega_{3/2} h^2 = (m_{3/2}/m_{\chi, \tilde{\tau}_1}) \Omega_{\chi, \tilde{\tau}_1} h^2$ . We recall that there are important cosmological and astrophysical constraints on long-lived NLSP decays, which we do not discuss here.

Concerning the LHC constraints, we note that  $M_h$  is always far below the LHC measurement, which is a much stronger constraint than that from the MET search. Both constraints are incompatible with the supersymmetric interpretation of  $g_\mu - 2$ . Since  $\tan\beta \leq 35$  in the portion of the mSUGRA  $(m_{1/2}, m_0)$  plane for  $A_0 = (3 - \sqrt{3}) m_0$  displayed in the left panel of Fig. 3, the  $B_s \rightarrow \mu^+\mu^-$  constraint has no impact.

The right panel of Fig. 3 shows a similar analysis for the case  $A_0 = 2 m_0$ . Comparing

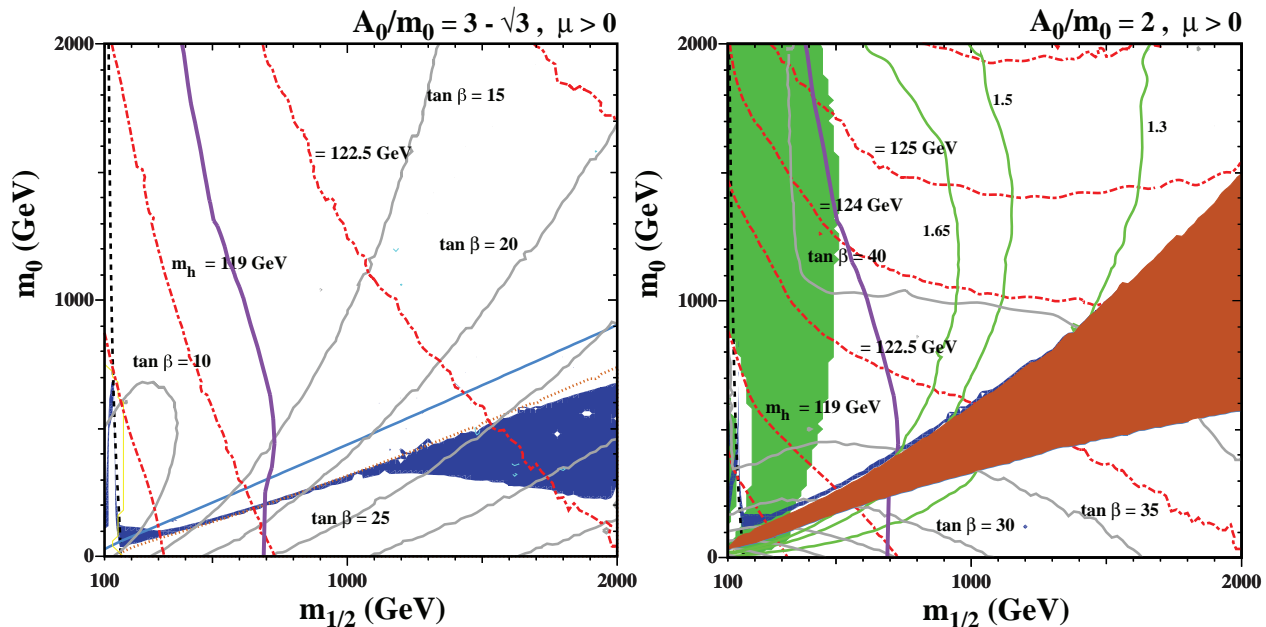


Figure 3: The  $mSUGRA$   $(m_{1/2}, m_0)$  planes for  $\mu > 0$  and  $A_0 = (3 - \sqrt{3})m_0$  (left),  $A_0 = 2m_0$  (right). The interpretations of the shading and contour colours are described in the text.

with the left panel, we see that the values of  $\tan \beta$  determined by the electroweak vacuum conditions are generally larger. For this reason, there is a region at low  $m_{1/2}$  that is excluded by  $b \rightarrow s\gamma$ , and the  $B_s \rightarrow \mu^+\mu^-$  constraint rules out a significant portion of the  $(m_{1/2}, m_0)$  plane. We also see that the LHC  $M_h$  constraint is respected for  $m_0 \gtrsim 1000$  GeV. In this case, there is a region where the stau is lighter than the lightest neutralino and both are lighter than the gravitino: this  $\tilde{\tau}_1$  LSP region is shaded dark brown. In the lower right wedge at large  $m_{1/2}$  and small  $m_0$ , below the brown excluded region, the gravitino is once again the LSP and the  $\tilde{\tau}_1$  is the NLSP. In this case, above the  $\tilde{\tau}_1$  LSP region, we do find a WMAP co-annihilation strip, which extends to  $m_{1/2} \sim 1100$  GeV. However, this strip has  $M_h \lesssim 123$  GeV and fails to respect the  $B_s \rightarrow \mu^+\mu^-$  constraint.

This summary serves to illustrate a broader incompatibility between the LHC constraints and  $mSUGRA$ , traceable to the extra constraints in this model compared to the CMSSM. We note that a more complete statistical analysis which included early LHC results already showed incompatibilities in the  $mSUGRA$  constructions [41].

## 4 The NUHM

### 4.1 Results for NUHM1 Models

We recall that the extra parameter introduced in the NUHM1 allows either  $m_A$  or  $\mu$  to be treated as a free parameter when solving the electroweak vacuum conditions (3, 4) for any set of fixed values of  $m_{1/2}, m_0, A_0$  and  $\tan \beta$ . Fig. 4 displays some representative  $(m_{1/2}, m_0)$

planes for fixed  $A_0$ ,  $\tan \beta$  and  $m_A$ , and Fig. 5 displays analogous planes for fixed values of  $\mu$ .

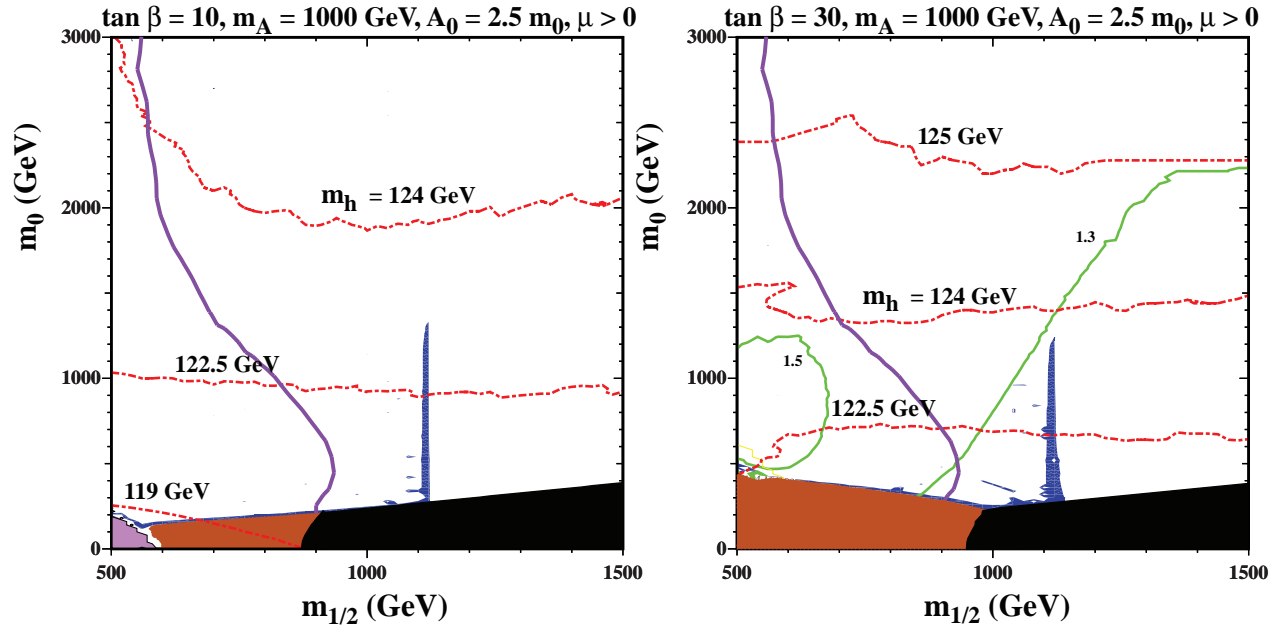


Figure 4: The NUHM1  $(m_{1/2}, m_0)$  planes for  $\mu > 0$ ,  $m_A = 1000$  GeV,  $A_0 = 2.5 m_0$  and  $\tan \beta = 10$  (left) and  $= 30$  (right). The interpretations of the shading and contour colours are described in the text.

When  $m_A$  is held fixed as in Fig. 4, one finds an s-channel rapid annihilation funnel at a value of  $m_{1/2}$  slightly greater than  $m_A$  (we recall that the funnel appears when  $2m_\chi \simeq m_A$ , and that  $m_\chi \sim 0.43m_{1/2}$ ). This is seen as a vertical structure at  $m_{1/2} \gtrsim 1100$  GeV<sup>5</sup> that is comfortably compatible with the LHC MET searches. For  $\tan \beta = 10$ , the funnel does not extend past  $M_h \simeq 123$  GeV, whereas it extends almost up to  $M_h = 124$  GeV for  $\tan \beta = 30$ . In both cases, the Higgs mass is probably too small to be compatible with the LHC result. Again, on the other hand, since the funnels shown here were chosen to occur at relatively large  $m_{1/2}$ , there is no conflict with the LHC MET searches. For  $\tan \beta = 30$ , the branching ratio of  $B_s \rightarrow \mu^+ \mu^-$  is somewhat higher than the Standard Model value, but it is still within the current 95% CL upper limit. At  $\tan \beta = 40$  (not displayed), there is increased tension with  $B_s \rightarrow \mu^+ \mu^-$  as the funnel sits very close to the 95% CL upper limit (a ratio of 1.5). In addition, at the higher value of  $\tan \beta$ , the end point of the funnel rises up only to 123 GeV.

Large regions of acceptable parameter space are found in the  $(m_{1/2}, m_0)$  plane when  $\mu$  is held fixed, as seen in Fig. 5 where  $\mu = 500$  GeV. Here we have again fixed  $\tan \beta = 10$  and  $A_0 = 2.5m_0$  in the left panel, but have taken  $\tan \beta = 40$  and  $A_0 = 2m_0$  in the right panel. For larger  $A_0/m_0$ , the  $\tilde{\tau}_1$  LSP region (shaded brown) collides with the region (shaded mauve) where there is no radiative electroweak symmetry breaking. At low  $m_{1/2}$ , there is a  $\tilde{\tau}_1$  coannihilation strip which has low  $M_h$  when  $\tan \beta = 10$ , and is for the most part in conflict with  $b \rightarrow s\gamma$  when  $\tan \beta = 40$ . At larger  $m_{1/2}$ , there is an increasing Higgsino component in

<sup>5</sup>The width of the structure is enhanced for visibility by colouring the area where  $0.06 < \Omega_\chi h^2 < 0.2$ .

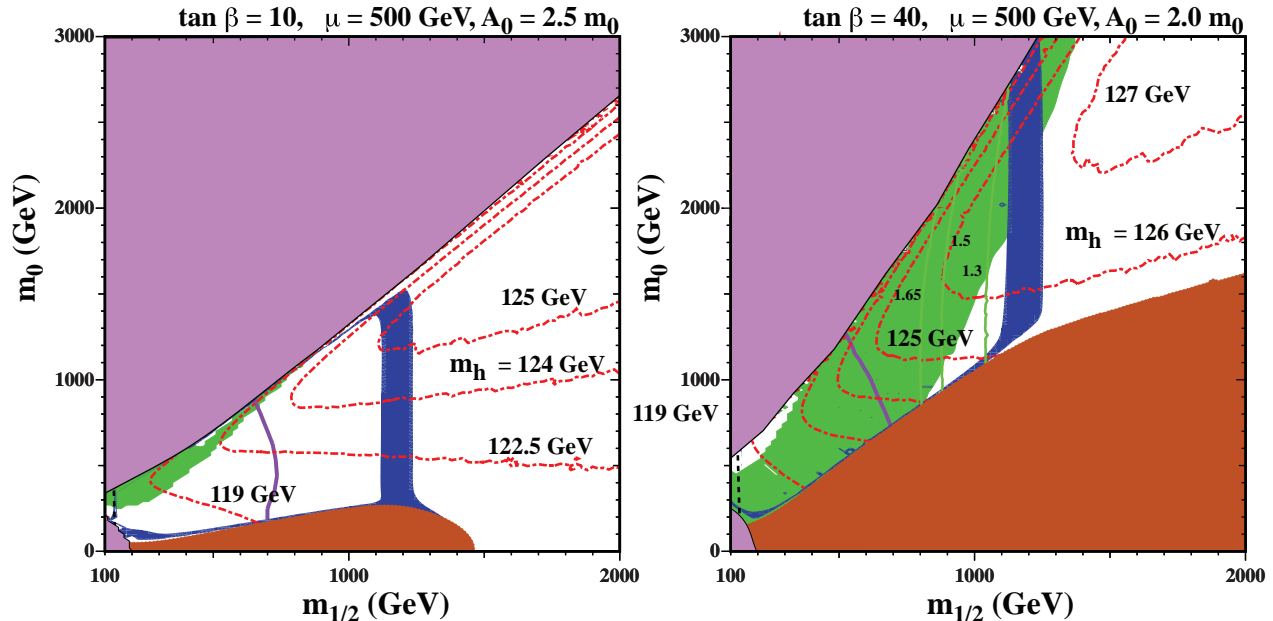


Figure 5: The NUHM1  $(m_{1/2}, m_0)$  planes for  $\mu > 0$ ,  $\mu = 500$  GeV,  $\tan\beta = 10$  and  $A_0 = 2.5 m_0$  (left) and  $\tan\beta = 40$  and  $A_0 = 2.0 m_0$  (right). The interpretations of the shading and contour colours are described in the text.

the LSP and, as result, an increased annihilation cross section. This results in the relatively thick vertical strips seen at  $m_{1/2} \sim 1200$  GeV in both panels, again comfortably consistent with the LHC MET searches, where the transition towards a Higgsino-like LSP causes the relic density to fall into the range favoured by WMAP. At still larger  $m_{1/2}$ , the relic  $\chi$  density is too small, but this region is not excluded if there is another dark matter candidate.

For the fixed parameter choices in Fig. 5, this transition strip lies beyond the current LHC MET search. In this case, it is possible to obtain a Higgs mass in excess of 125 GeV even for  $\tan\beta = 10$ , and much of the transition strip lies in excess of  $M_h = 126$  when  $\tan\beta = 40$ . As seen from the contours showing the branching ratio of  $B_s \rightarrow \mu^+ \mu^-$ , this region is also compatible with the recent LHCb result.

There are of course many possible slices that one can make through the NUHM1 parameter space, and we only show a few of the more interesting ones here. In Fig. 6, we show examples of  $(\mu, m_{1/2})$  planes with fixed  $m_0 = 1000$  GeV and  $A_0 = 2.5 m_0$ ,  $\tan\beta = 10$  on the left and  $\tan\beta = 30$  on the right. In both panels there is a brown shaded region at low  $m_{1/2}$  and small  $|\mu|$  corresponding to a stop LSP (or even a tachyonic stop). Just above the shaded region, there is a thin strip where the relic density falls in the WMAP range due to stop co-annihilations. However, if it is not excluded by  $b \rightarrow s\gamma$ , the value of  $M_h$  is too low. Jutting out from this region, are two antenna-like strips with  $m_{1/2} \gtrsim 800$  GeV and hence compatible with the LHC MET constraint, which correspond again to the transition between bino and Higgsino-like LSPs we met in the previous figure. In the region between the two antennae, the relic density is too small. For  $\tan\beta = 10$ ,  $M_h$  is in excess of 124 GeV, and for  $\tan\beta = 30$ , it is in excess of 125 GeV. For  $\tan\beta = 30$ , the brown shaded regions at

large  $m_{1/2}$  depict regions with a  $\tilde{\tau}_1$  LSP. At still higher  $\tan \beta$ , these would descend and cover much of the plane.

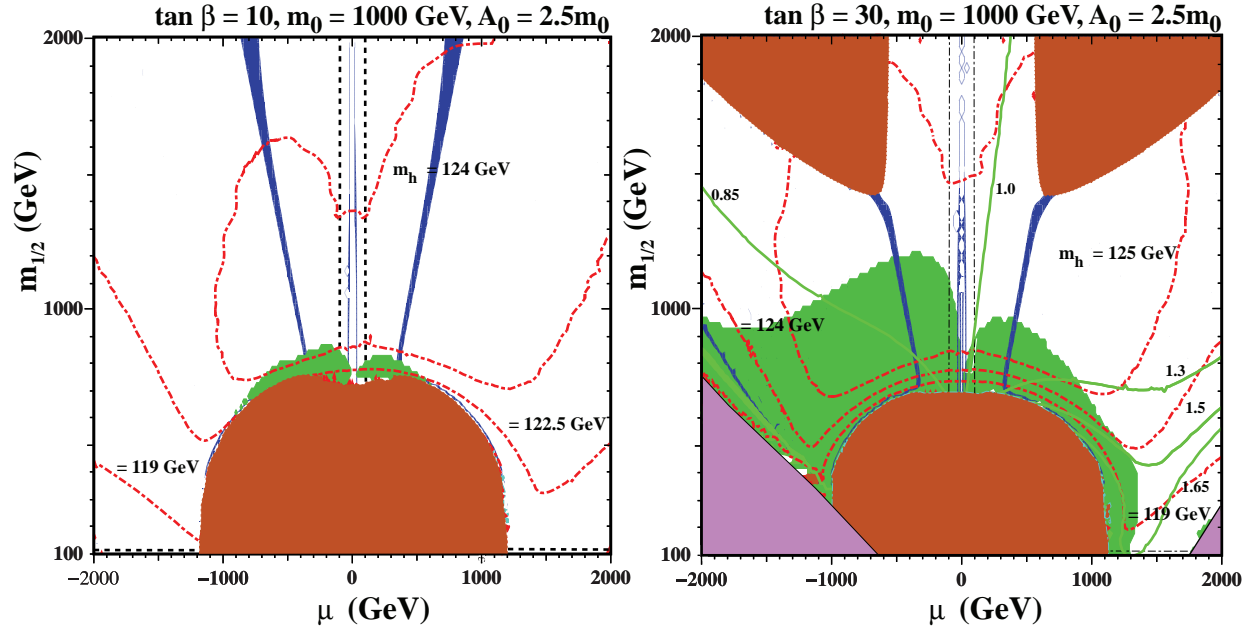


Figure 6: The NUHM1  $(\mu, m_{1/2})$  planes for  $m_0 = 1000 \text{ GeV}$ ,  $A_0 = 2.5 m_0$ , and  $\tan \beta = 10$  (left) and  $\tan \beta = 30$  (right). The interpretations of the shading and contour colours are described in the text.

It is interesting to note that in the right panel of Fig. 6 the branching ratio of  $B_s \rightarrow \mu^+ \mu^-$  falls below the Standard Model value, particularly when  $\mu < 0$ . Here we find a region with acceptable relic LSP density, a Higgs mass  $M_h \simeq 125.5 \text{ GeV}$ , acceptable  $b \rightarrow s \gamma$ , and  $B_s \rightarrow \mu^+ \mu^-$  at 0.9 its Standard Model value, close to the central value measured by LHCb.

In Fig. 7 we show one more example of NUHM1 planes, a pair of  $(\mu, m_0)$  planes with fixed  $m_{1/2} = 1000 \text{ GeV}$  (and hence LHC MET-compatible) and  $A_0 = 2.5 m_0$ , with  $\tan \beta = 10$  on the left and  $\tan \beta = 30$  on the right. We again find regions with either a  $\tilde{t}_1$  LSP (high  $m_0$ ) or a  $\tilde{\tau}_1$  LSP (low  $m_0$ ) with corresponding adjacent  $\tilde{t}_1$  or  $\tilde{\tau}_1$  coannihilation strips. These coannihilation strips have either a low Higgs mass or are in conflict with  $b \rightarrow s \gamma$ . At larger values of  $|\mu|$  we also see regions where sleptons of the first two generations can become the LSP (coloured black). In both panels, there are vertical transition strips with suitably large values of  $M_h$ . The constraint from  $b \rightarrow s \gamma$  becomes particularly strong for  $\mu < 0$  and  $\tan \beta = 30$ , while the transition strip for  $\mu > 0$  has a branching fraction for  $B_s \rightarrow \mu^+ \mu^-$  close to the Standard Model prediction.

These examples illustrate that the NUHM1 has the flexibility to accommodate the LHC constraints in a quite generic way, exploiting the extra flexibility in the Higgs sector of this model.

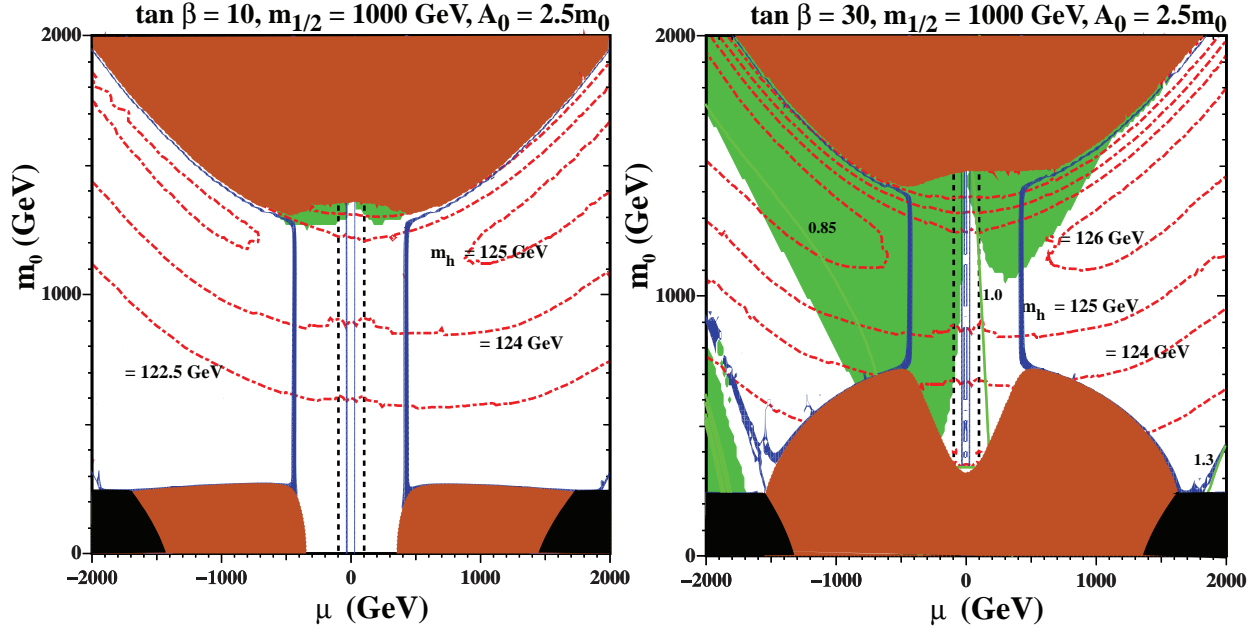


Figure 7: The NUHM1  $(\mu, m_0)$  planes for  $m_{1/2} = 1000$  GeV,  $A_0 = 2.5m_0$ , and  $\tan\beta = 10$  (left) and  $\tan\beta = 30$  (right). The interpretations of the shading and contour colours are described in the text.

## 4.2 Results for NUHM2 Models

There are still more planes that can be constructed in the NUHM2, with its extra free parameter. Here we show only one pair of  $(\mu, m_A)$  planes that are LHC MET-compatible, with fixed  $m_{1/2} = m_0 = 1000$  GeV and  $A_0 = 2.5m_0$  and, as in previous planes,  $\tan\beta = 10$  on the left and  $\tan\beta = 30$  on the right. In both these particular examples, we see cruciform regions of acceptable relic density formed by the combination of a funnel, around fixed  $m_A \simeq 900$  GeV, and a transition to a Higgsino LSP when  $|\mu| \lesssim 500$  GeV. The constraint from  $b \rightarrow s\gamma$  disfavors more of the parameter space with  $\mu < 0$ , particularly when  $\tan\beta = 30$ . For this value of  $\tan\beta$ , the constraint from  $B_s \rightarrow \mu^+\mu^-$  excludes the surviving portions of the relic density strips below  $m_A \approx 1000$  GeV when  $\mu > 0$ . However, at large  $m_A$ ,  $\text{BR}(B_s \rightarrow \mu^+\mu^-)$  is sufficiently small and  $M_h \simeq 125$  GeV. In the case of  $\tan\beta = 10$ ,  $M_h \gtrsim 124$  GeV for most of the cruciform region of acceptable relic density, and  $B_s \rightarrow \mu^+\mu^-$  has no significant impact.

These two examples illustrate that the extra degree of freedom in the NUHM2 opens up even broader possibilities for reconciling supersymmetry with the LHC constraints.

## 5 Results for sub-GUT CMSSM models

We now consider a different one-parameter extension, one in which the soft supersymmetry-breaking parameters  $m_{1/2}, m_0$  and  $A_0$  are assumed to be universal at some input scale  $M_{in}$  below the conventional supersymmetric GUT scale, as might arise in models where the supersymmetry-breaking dynamics acts below the GUT scale. As was discussed in [21] and

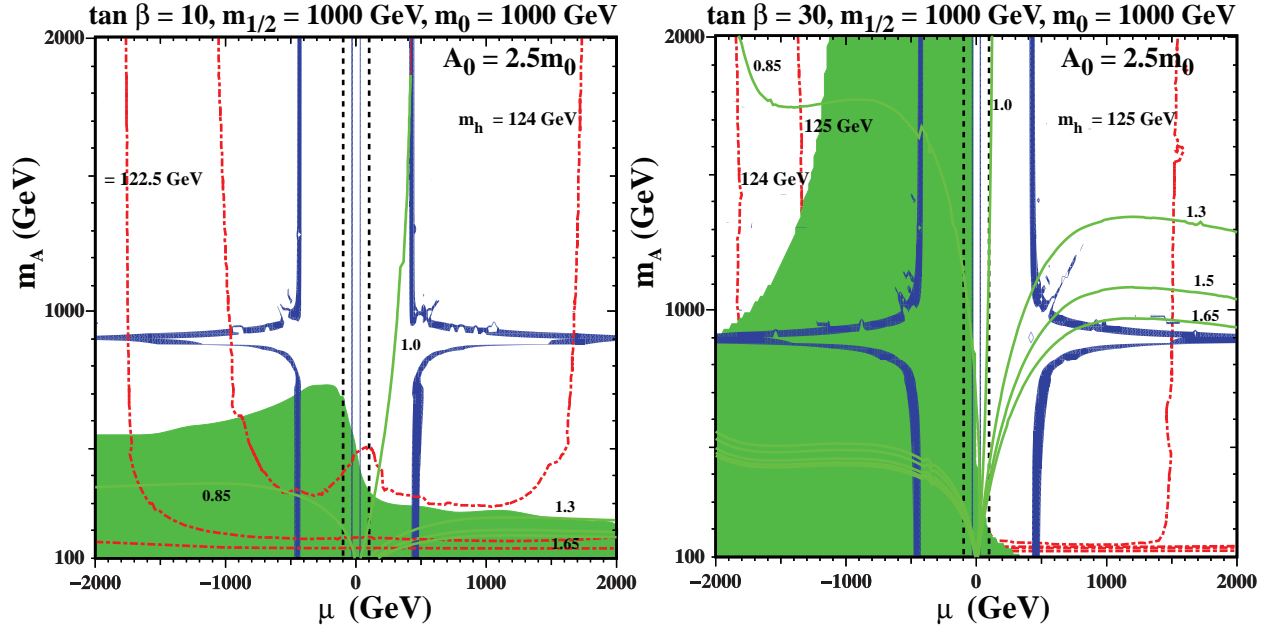


Figure 8: The NUHM2  $(\mu, m_A)$  planes for  $m_{1/2} = 1000$  GeV,  $m_0 = 1000$  GeV,  $A_0 = 2.5 m_0$ , and  $\tan \beta = 10$  (left) and  $\tan \beta = 30$  (right). The interpretations of the shading and contour colours are described in the text.

summarized earlier, the sparticle spectrum in such a scenario is in general more compressed than in the conventional CMSSM with, e.g., smaller mass differences between squarks and sleptons and between different types of inos. Models with similarly compressed spectra and the prospects for their discovery have been studied in [42].

As presented in [21], this compression of the spectrum causes the relic cold dark matter density to decrease at generic fixed values of  $(m_{1/2}, m_0)$  as  $M_{in}$  decreases, and hence the strips of parameter space with the appropriate dark matter density tend to move inwards from the boundary of the region allowed by the neutral LSP and electroweak symmetry breaking constraints. These features are visible in the upper panels of Fig. 9, which are  $(m_{1/2}, m_0)$  planes for  $\tan \beta = 10$  and 40, both with  $M_{in} = 10^{11}$  GeV,  $A_0 = 2.5 m_0$ , and  $\mu > 0$ . In both cases there are wedges of the  $(m_{1/2}, m_0)$  plane at small  $m_{1/2}$  and large  $m_0$  (and hence large  $A_0$ ) that are excluded because the lighter stop,  $\tilde{t}_1$ , is the LSP in addition to the common wedge in the lower right of the planes where there is a  $\tilde{\tau}_1$  LSP. We see that in both panels there is a prominent funnel due to s-channel annihilations of LSPs through the heavy Higgs scalar and pseudoscalar, where the relic cold dark matter density is suitable. There are also other very thin strips running above and roughly parallel to the prominent funnels, due to rapid s-channel *coannihilation* processes between the LSP and heavier neutralinos and charginos. In both cases, we also see  $\tilde{t}_1$  coannihilation strips near the upper boundary of the allowed  $\chi$  LSP region, in the neighbourhood where focus-point strips appear in the CMSSM.

We now discuss how these sub-GUT models fare with the available LHC constraints. The MET constraint (not shown) excludes only a small corner of the displayed triangle between the  $\tilde{\tau}_1$  and  $\tilde{t}_1$  LSP boundaries. As usual,  $B_s \rightarrow \mu^+ \mu^-$  does not impact the allowed parameter

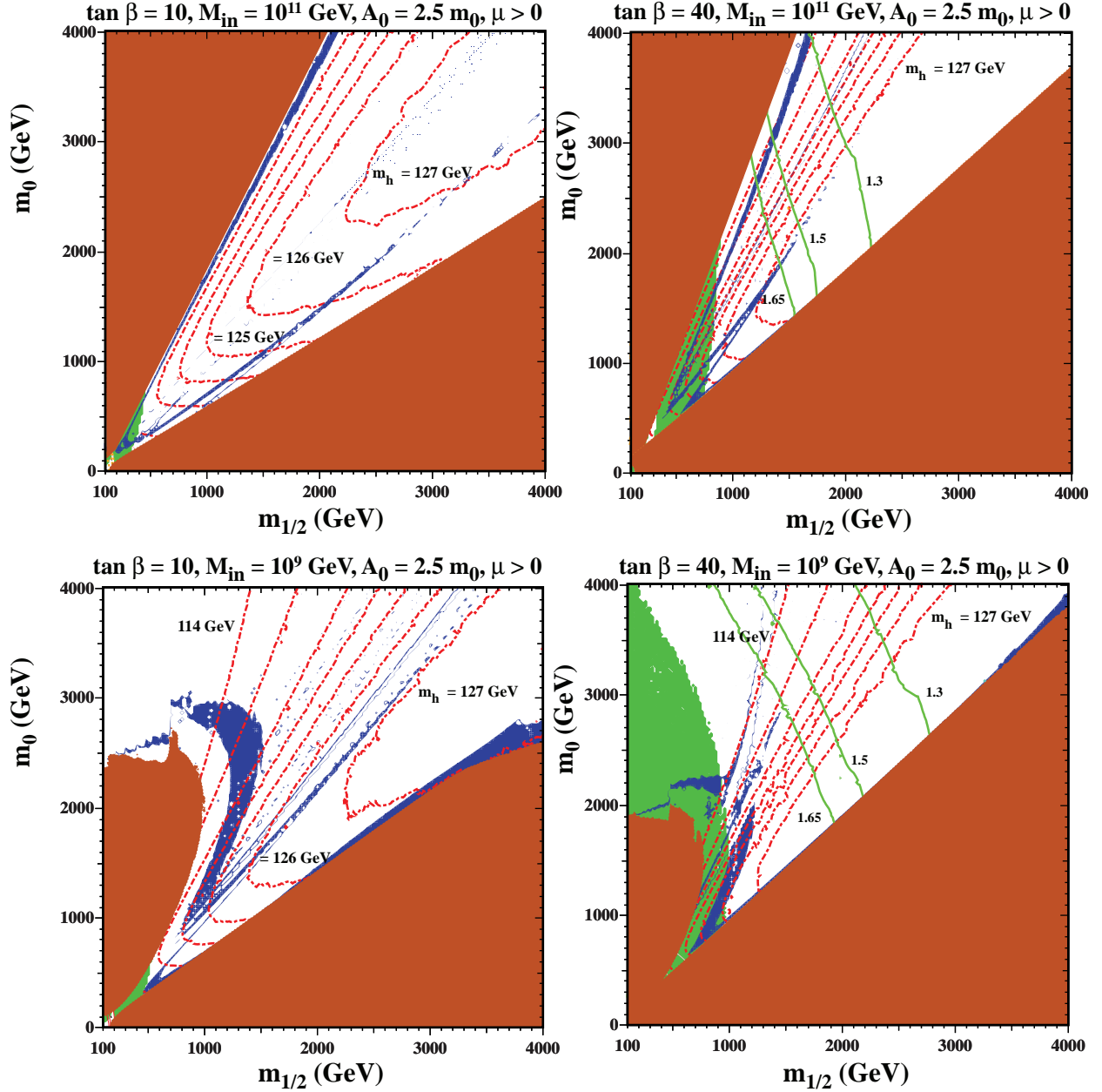


Figure 9: *Sub-GUT CMSSM scenarios with  $\tan \beta = 10$  (left) and  $\tan \beta = 40$  (right) in both cases with  $A_0 = 2.5 m_0$ , and for  $M_{\text{in}} = 10^{11} \text{ GeV}$  (upper) and  $10^9 \text{ GeV}$  (lower). Plotted contours of  $M_h$  are 114, 119, 122.5, 124, 125, 126, and 127 GeV. The interpretations of the shading and contour colours are described in the text.*

space for  $\tan \beta = 10$ , but does have significant impact for  $\tan \beta = 40$ , requiring  $m_{1/2} \gtrsim 1500$  to 2000 GeV along the prominent rapid-annihilation funnel, and  $m_{1/2} \gtrsim 1000$  to 1500 GeV along the stop coannihilation strip. The most novel feature of these sub-GUT models is the relative ease with which they respect the Higgs mass constraint. Most of the funnel for



$\tan\beta = 10$  is compatible with  $M_h = 125$  to  $126$  GeV, once the uncertainties in the theoretical calculation within the CMSSM are taken into account. This is also true along the funnel when  $\tan\beta = 40$ , for the points compatible with  $B_s \rightarrow \mu^+\mu^-$ . On the other hand, in both cases the value of  $M_h$  is too small along the stop coannihilation strip.

The lower panels of Fig. 9 display  $(m_{1/2}, m_0)$  planes for the same values of  $\tan\beta$ ,  $\mu > 0$  and  $A_0 = 2.5 m_0$ , but now with  $M_{in} = 10^9$  GeV. In each case, rotating anticlockwise around the plane from the lower right, we first see a stau coannihilation strip followed by a rapid-annihilation funnel (which are both more prominent for  $\tan\beta = 10$ ). In the  $\tan\beta = 10$  case (lower left) we also see ‘echo’ funnel strips where  $m_{1/2}$  is smaller for the same value of  $m_0$ , which are due to s-channel coannihilations between the LSP and more massive neutralinos and charginos. At lower  $M_{in}$ , there is less running and stops remain heavier than the lightest neutralino at lower  $m_0$ , thus, we see a recession of the stop LSP region at lower  $M_{in}$ . Next to this region, we see a prominent stop coannihilation strip, but note that only for small  $m_0$  does it have an acceptable value of  $M_h$ . In the  $\tan\beta = 40$  case, the s-channel funnels merge with the stop coannihilation strip for  $(m_{1/2}, m_0) \sim (1000, 2000)$  GeV (adjacent to a region excluded by  $b \rightarrow s\gamma$ ), again yielding acceptable  $M_h$  for lower  $m_0$ . The LHC MET constraint is not relevant in either of the lower planes, and neither is  $B_s \rightarrow \mu^+\mu^-$  when  $\tan\beta = 10$ . However,  $B_s \rightarrow \mu^+\mu^-$  does exclude almost all the dark matter regions for  $\tan\beta = 40$ , with the exception of the stau coannihilation strip which reemerges at very large  $m_{1/2}$ .

These examples illustrate how sub-GUT CMSSM models are better able to accommodate the LHC constraints, principally because the greater importances of additional (co)annihilation processes permit larger values of  $m_{1/2}$  and  $m_0$  than in the conventional GUT-scale CMSSM.

## 6 Results for sub-GUT mSUGRA models

Encouraged by the relative success of sub-GUT CMSSM models in accommodating the latest LHC constraints together with other constraints, we now consider whether this compatibility can be maintained if we remove one of the sub-GUT CMSSM parameters by imposing the mSUGRA relation between the trilinear and bilinear soft supersymmetry-breaking parameters:  $A_0 = B_0 + m_0$ , and also the mSUGRA relation between the gravitino and scalar masses:  $m_{3/2} = m_0$  before renormalization.

We start with the  $(m_{1/2}, m_0)$  planes for the Polonyi case  $A_0 = (3 - \sqrt{3})m_0$  shown in Fig. 10. (Results for a GUT-scale Polonyi model were shown in the left panel of Figure 3.) The case  $M_{in} = 10^{13}$  GeV is displayed in the upper left panel of Fig. 10, where we see that there is a forbidden region at large  $m_{1/2}$  and  $m_0 \sim 2000$  GeV where the  $\tilde{\tau}_1$  is the LSP. At larger  $m_0$  and/or smaller  $m_{1/2}$  the lightest neutralino  $\chi$  is the LSP, and at smaller  $m_0$  the gravitino is the LSP. There is a narrow funnel in the  $\chi$  LSP region with suitable cold dark matter density that barely reaches  $(m_{1/2}, m_0) \sim (2000, 1500)$  GeV, and a ‘boomerang’ region at lower  $m_0$ , extending to large  $m_{1/2}$ , where the density of gravitino LSPs produced in NLSP decays is suitable for the cold dark matter. The tip of the  $\chi$  LSP funnel and the upper arm of the gravitino boomerang are just barely compatible with  $M_h \sim 124$  GeV, which is

compatible with the LHC measurement within uncertainties. We note that all (most of) the visible part of the plane is compatible with the LHC  $B_s \rightarrow \mu^+\mu^-$  (MET) constraint, including these two  $M_h$ -compatible regions. In this plane,  $\tan\beta$  is relatively small except when  $m_{1/2}$  is very large. This accounts for the sufficiently low value of  $B_s \rightarrow \mu^+\mu^-$  relative to the Standard Model (between 1.0 and 1.3 over much of the displayed plane).

Turning now to the upper right panel of Fig. 10 for  $M_{in} = 10^{11.5}$  GeV, and descending from the boundary of the electroweak symmetry breaking region in the upper left to lower right, across the  $\chi$  LSP region, we encounter several new dark matter-compatible strips, some of which were present embryonically in previous figures. The uppermost in a series of wisps is due to  $\chi_3 - \chi^\pm$  coannihilation enhanced by a near-on-shell t-channel pole. Moving across the plane towards larger  $m_{1/2}$ , several wisps are crossed prior to reaching the most prominent diagonal feature, which is the more familiar  $\chi - \chi$  s-channel funnel. These wispy features above the  $\chi - \chi$  funnel are due to coannihilations of neutralinos and charginos enhanced by s-channel  $H/A$  poles. Further down and to the right there is a coannihilation strip adjacent to the forbidden  $\tilde{\tau}_1$  LSP triangle. Continuing below this triangle, we encounter a near-horizontal band where  $\tilde{\tau}_1$  decays yield a suitable density of gravitino LSPs. In this case, almost all the  $(m_{1/2}, m_0)$  plane is compatible with the LHC MET and  $B_s \rightarrow \mu^+\mu^-$  constraints, and large parts of the many dark matter-compatible strips in the  $\chi$  LSP region are compatible with the  $M_h$  measurement.

To help understand the origin of the multiple avenues for coannihilation, we show in the upper left panel of Fig. 11 the sparticle spectrum as a function of  $m_{1/2}$  for fixed  $m_0 = 2000$  GeV for  $M_{in} = 10^{11.5}$  GeV. Here we see clearly the possibility of multiple resonant reactions when  $m_A/2$  is equal to  $m_{\chi_3}$  at  $m_{1/2} \approx 800$  GeV,  $m_{\chi_2}$  at  $m_{1/2} \approx 1100$  GeV, and  $m_\chi$  at  $m_{1/2} \approx 1800$  GeV. In the upper right panel of Fig. 11, we see the behaviour of the neutralino composition as a function of the universal gaugino mass: the Higgsino composition is enhanced at large  $m_{1/2}$ , contributing to an increased cross section and hence acceptable relic density past the point where the stau coannihilation strip would normally end.

Looking back at the  $(m_{1/2}, m_0)$  plane for  $M_{in} = 10^{10.5}$  GeV shown in the lower left panel of Fig. 10, and again descending across the  $\chi$  LSP region away from the electroweak symmetry breaking boundary towards the  $\tilde{\tau}_1$  LSP region, we again encounter several near-parallel dark matter-compatible strips. The first is a relatively broad focus-point region where the LSP is more Higgsino-like, then there is a coannihilation funnel, followed by the more familiar  $\chi - \chi$  rapid-annihilation funnel. Finally, we encounter a Higgsino -  $\tilde{\tau}_1$  coannihilation strip. Below the  $\tilde{\tau}_1$  LSP region, there is again a band where  $\tilde{\tau}_1$  NLSP decays to gravitinos yield a suitable relic dark matter density. As in the previous case, most of the  $(m_{1/2}, m_0)$  plane is again compatible with the LHC MET and  $B_s \rightarrow \mu^+\mu^-$  constraints due to the relatively large mass scales and/or small value of  $\tan\beta$ . The upper parts ( $m_0 \gtrsim 2$  TeV) of the dark matter-compatible strips in the  $\chi$  LSP region are compatible with the  $M_h$  measurement.

Finally, we consider the  $(m_{1/2}, m_0)$  plane for  $M_{in} = 10^{10}$  GeV shown in the lower right panel of Fig. 10. At large  $m_0$ , we see that the broad focus-point strip is joined to one side of the standard  $\chi - \chi$  funnel. The other side of this funnel is connected to a Higgsino coannihilation strip hovering above the  $\tilde{\tau}_1$  LSP boundary. At lower  $m_0$  and  $m_{1/2}$ , there is another loop connecting the lower part of the focus-point strip with the  $\chi - \chi$  funnel, and at

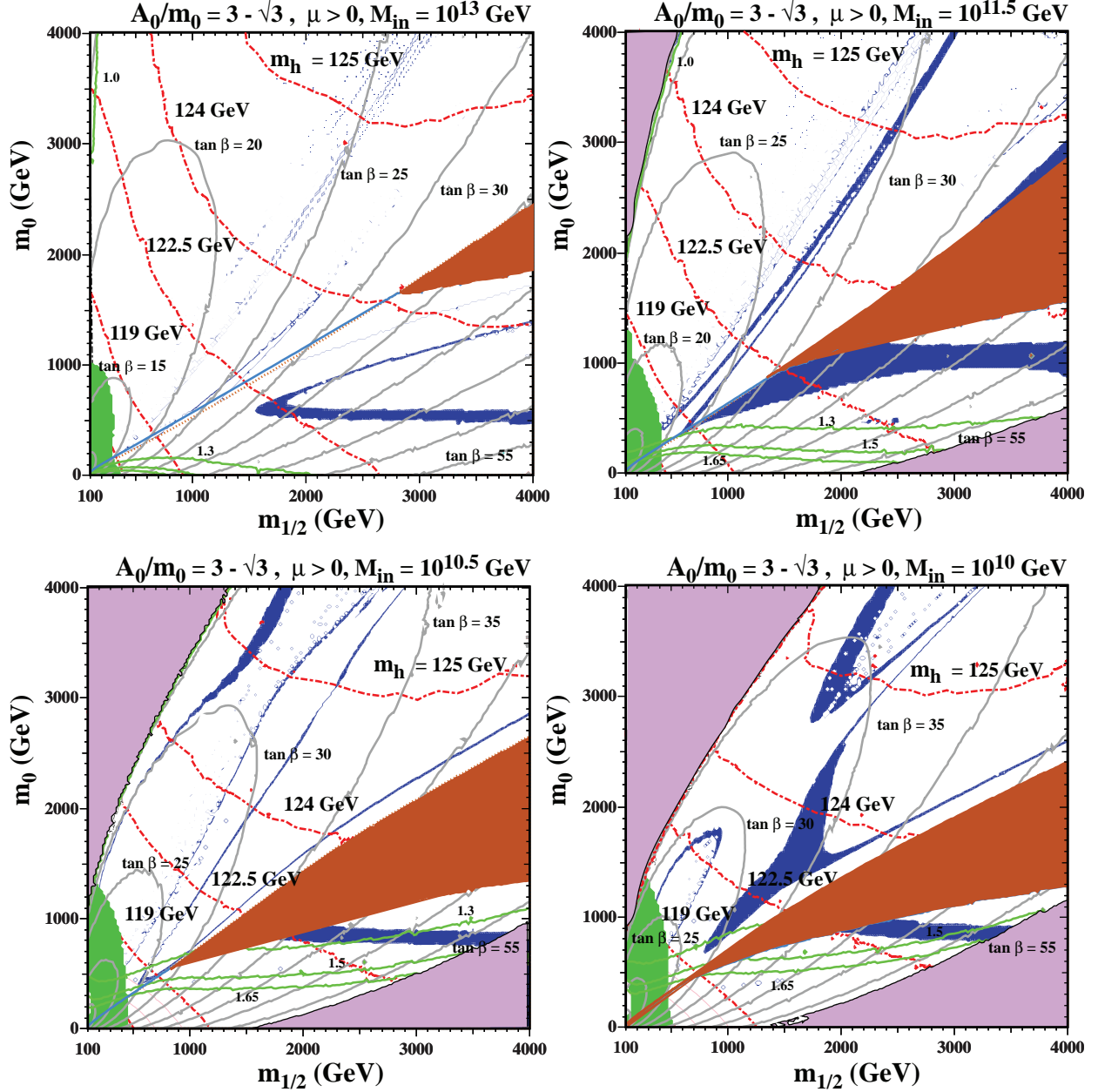


Figure 10: The  $(m_{1/2}, m_0)$  planes for  $\mu > 0$  in the sub-GUT Polonyi  $mSUGRA$  model with  $A_0 = (3 - \sqrt{3})m_0$  and  $M_{in} = 10^{13}$  GeV (upper left),  $10^{11.5}$  GeV (upper right),  $10^{10.5}$  GeV (lower left) and  $10^{10}$  GeV (lower right), found using the latest version of the SSARD code [38]. The interpretations of the shadings and contour colours are described in the text.

low  $m_0$  but larger  $m_{1/2}$  there is again a band where gravitinos could provide the dark matter. As before, most of the  $(m_{1/2}, m_0)$  plane is compatible with the LHC MET and  $B_s \rightarrow \mu^+ \mu^-$  constraints, and there are large stretches of the dark matter strips at large  $m_{1/2}$  and  $m_0$  that are compatible with the LHC Higgs measurement.

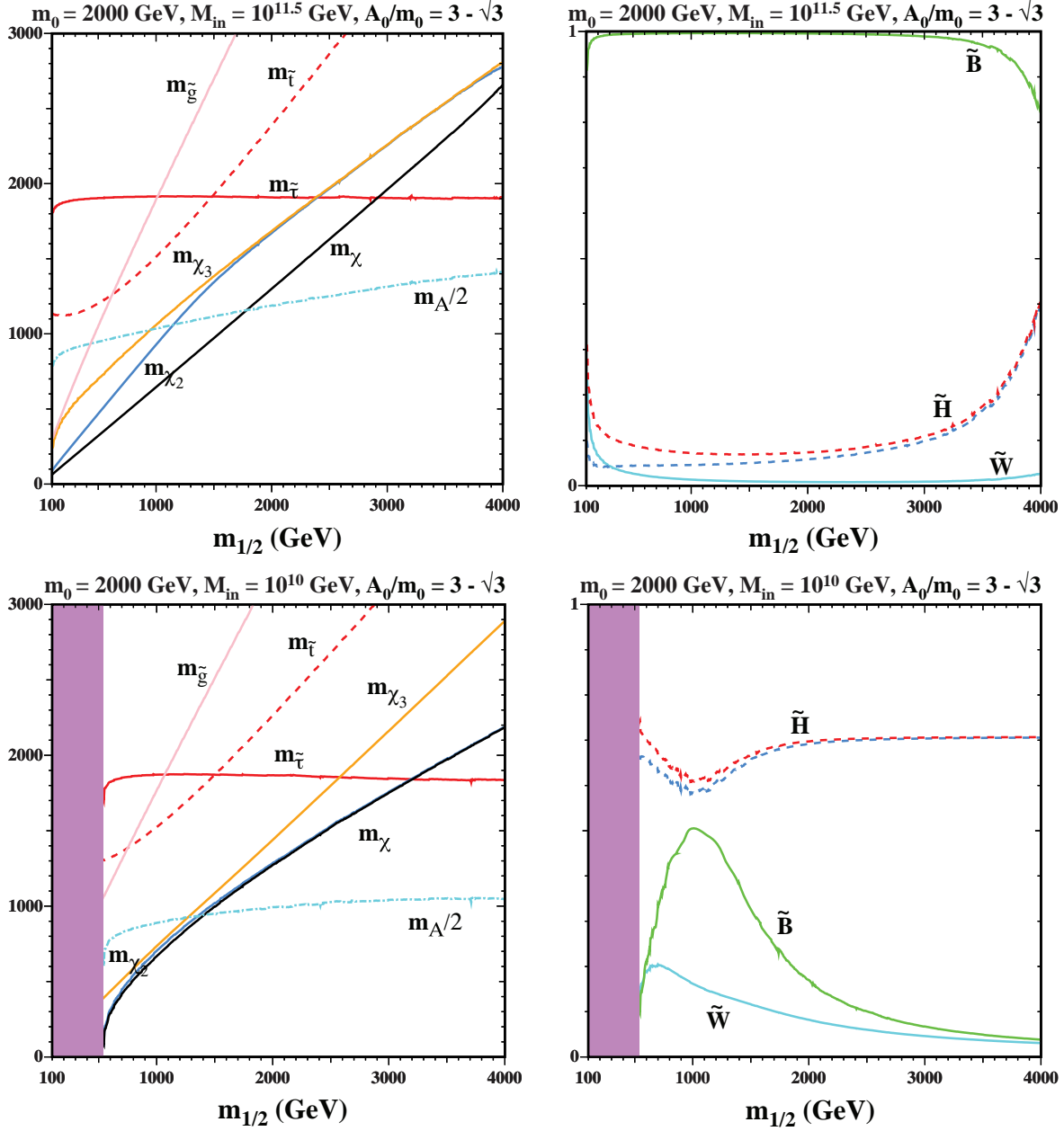


Figure 11: *The sparticle spectrum (left panels) and (right panels) the composition of the LSP  $\tilde{\chi}$  as functions of  $m_{1/2}$  in a sub-GUT Polonyi mSUGRA scenario with  $m_0 = 2000 \text{ GeV}$ , for  $M_{in} = 10^{11.5} \text{ GeV}$  (upper panels) and  $10^{10} \text{ GeV}$  (lower panels).*

For this case also, we display the sparticle masses and neutralino composition as functions of  $m_{1/2}$  for  $m_0 = 2000 \text{ GeV}$  in the lower panels of Figure 11. Here, we clearly see the congruence of masses at  $m_{1/2} \approx 1000 \text{ GeV}$  all contributing to a resulting low relic density. In this case, we also see that, for this value of  $m_0$ , the neutralino is predominantly a Higgsino, but in the funnel centre, there is an enhanced bino component leading to a very mixed LSP

which also leads in general to an enhanced cross section.

The above discussion was for sub-GUT Polonyi mSUGRA models, and we now discuss briefly what happens in sub-GUT mSUGRA models with values of  $A_0 \neq (3 - \sqrt{3})m_0$ . First, we recall that in mSUGRA models the value of  $\tan \beta$  is fixed by the electroweak conditions as a function of the other, independent model parameters, as shown by the grey contours in the different panels of Fig. 10. As shown there, in the Polonyi case typical values are  $\tan \beta \sim 20$  to 30, which is why the  $B_s \rightarrow \mu^+\mu^-$  has relatively little impact - though this does increase slightly at smaller  $M_{in}$  where larger values of  $\tan \beta$  are found. On the other hand, we have already seen in the right panel of Fig. 3 that the derived values of  $\tan \beta$  are as large as  $\sim 40$  for  $M_{in} = M_{GUT}$ .

In sub-GUT mSUGRA models with  $A_0 = 2m_0$ , as shown in Fig. 12, we see that  $\tan \beta$  increases to  $\sim 45$  to 50 for  $M_{in} = 10^{14}$  and  $10^{13}$  GeV. This has two consequences worth noting: (i) the impact of the  $B_s \rightarrow \mu^+\mu^-$  constraint is increased to such an extent, compared to the Polonyi case, that no  $A_0 = 2m_0$  sub-GUT mSUGRA models are valid for either value of  $M_{in}$ , and (ii) for  $M_{in} < 10^{13}$  GeV, the increasing value of  $\tan \beta$  induces non-perturbative instabilities in the renormalization-group equations over much of the  $(m_{1/2}, m_0)$  plane. For these reasons, sub-GUT mSUGRA models with  $A_0$  much larger than the Polonyi value are disfavoured.

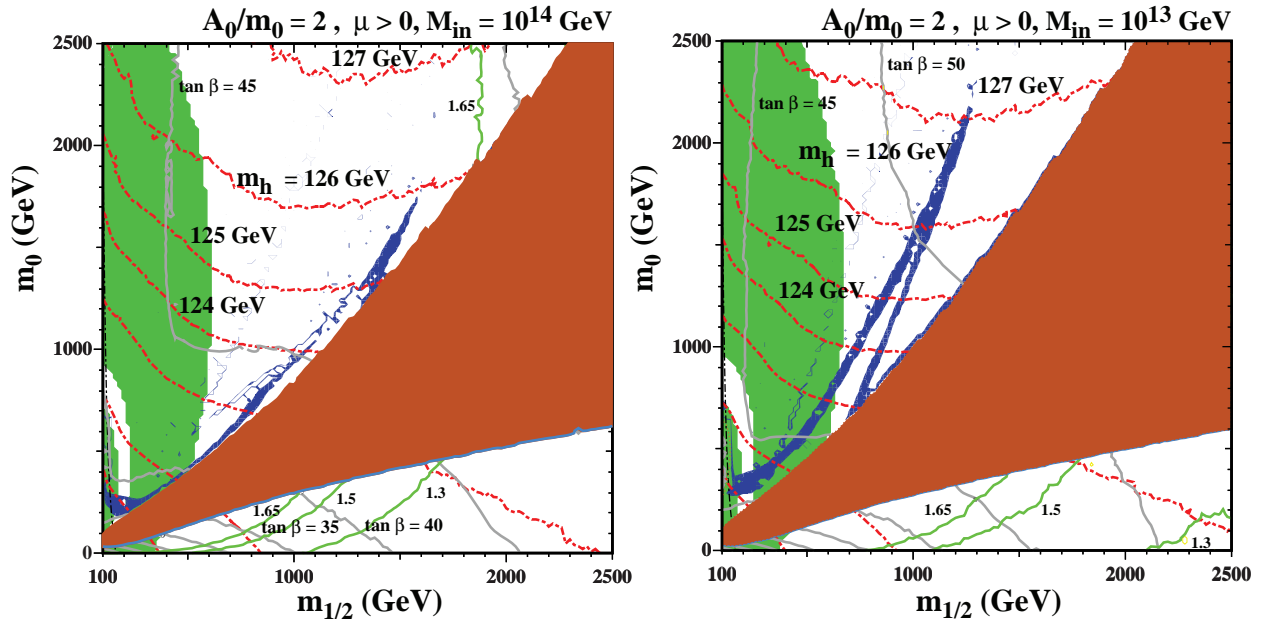


Figure 12: The sub-GUT mSUGRA  $(m_{1/2}, m_0)$  planes for  $A_0 = 2m_0$  and  $M_{in} = 10^{14}$  GeV (left),  $M_{in} = 10^{13}$  GeV (right). The interpretations of the shading and contour colours are described in the text.

In the case of sub-GUT mSUGRA models with  $A_0$  less than the Polonyi value, we recall (see also the left panel of Fig. 3), that  $M_h$  is much smaller than the LHC measurement if  $A_0 = 0$  and  $M_{in} = M_{GUT}$ . This problem persists for  $M_{in} < M_{GUT}$ , so we do not discuss further this possibility.

The key messages from this study are that (i) many (co)annihilation processes that are relatively unimportant in the CMSSM can become important in sub-GUT models, as the sparticle spectrum becomes more degenerate and Boltzmann suppression factors therefore become less significant. As a result, (ii) the cold dark matter density may fall into the favoured range almost anywhere in the interior of the  $(m_{1/2}, m_0)$  plane away from the  $\tilde{\tau}_1$  LSP and electroweak symmetry breaking boundaries, depending on the precise value of  $M_{in}$  and  $A_0$ . Next, (iii) many of the regions allowed by the dark matter constraint are compatible with the current LHC constraints, including the  $M_h$  measurement. Finally and intriguingly, (iv) in the specific cases of sub-GUT mSUGRA models, values of  $A_0$  very different from the Polonyi value  $A_0 = (3 - \sqrt{3}) m_0$  are disfavoured.

## 7 Summary

It is well known that only very small regions of the CMSSM parameter space are consistent with all the theoretical, phenomenological, experimental, astrophysical and cosmological constraints, notably including the preferred range of the cold dark matter density. We have explored in this paper the extent to which some generalizations of the CMSSM may wriggle out of the straitjacket imposed, in particular, by the LHC constraint on missing-energy (MET) events, by the LHCb measurement of the branching ratio for  $B_s \rightarrow \mu^+ \mu^-$  and the LHC measurement of the mass of the Higgs boson. The principal classes of models studied are those with non-universal supersymmetry-breaking contributions to the Higgs masses (NUHM1,2) and models in which universality is imposed on the supersymmetry-breaking parameters at some input scale  $M_{in} < M_{GUT}$  (sub-GUT CMSSM and mSUGRA).

It is not difficult to find regions of the NUHM1,2 parameter spaces where the cosmological cold dark matter density falls within the preferred range, even if the sparticle masses are relatively large, as required by the LHC MET and  $M_h$  constraints. For example, this may happen in a transition region where the  $\chi$  LSP has a relatively large Higgsino component. In the CMSSM, this could happen only in the focus-point region, a possibility now disfavoured by the XENON100 upper limit on cold dark matter scattering, but in the NUHM1 the  $\mu$  parameter may be regarded as free and the transition region may appear in other parts of the  $(m_{1/2}, m_0)$  plane where the LHC MET and  $M_h$  constraints are respected and  $\text{BR}(B_s \rightarrow \mu^+ \mu^-)$  is close to the Standard Model value.

Sub-GUT models offer other possibilities for reconciling the LHC and other constraints. The compression of the spectrum as  $M_{in}$  decreases implies that more coannihilation processes may become important, suppressing the relic density below the range expected in the CMSSM, and enabling it to be compatible with the cosmological constraint also at relatively large values of  $m_{1/2}$  and  $m_0$ . Also, in sub-GUT models we find a proliferation of strips where the dark matter density falls within the preferred range.

The NUHM1,2 and sub-GUT models are examples to illustrate that there is no general conflict between the LHC constraints and supersymmetry, even within the MSSM framework. It suffices to relax the constraint of universality of the soft supersymmetry-breaking parameters at the GUT scale, as we have demonstrated in a few types of scenarios. However, it is worth noting that the surviving models in these particular scenarios tend to have

quite large sparticle masses, and do not provide a supersymmetric resolution of the  $g_\mu - 2$  discrepancy.

## Acknowledgments

The work of J.E. and F.L. was supported in part by the London Centre for Terauniverse Studies (LCTS), using funding from the European Research Council via the Advanced Investigator Grant 267352: this also supported visits by K.A.O. to the CERN TH Division, which he thanks for its hospitality. The work of F.L. and K.A.O. was supported in part by DOE grant DE-FG02-94ER-40823 at the University of Minnesota, and the work of F.L. was also supported in part by a Doctoral Dissertation Fellowship at the University of Minnesota. P.S. gratefully acknowledges support and resources from the Center for High Performance Computing at the University of Utah.

## References

- [1] M. Drees and M. M. Nojiri, Phys. Rev. D **47** (1993) 376 [arXiv:hep-ph/9207234]; H. Baer and M. Brhlik, Phys. Rev. D **53** (1996) 597 [arXiv:hep-ph/9508321]; Phys. Rev. D **57** (1998) 567 [arXiv:hep-ph/9706509]; H. Baer, M. Brhlik, M. A. Diaz, J. Ferrandis, P. Mercadante, P. Quintana and X. Tata, Phys. Rev. D **63** (2001) 015007 [arXiv:hep-ph/0005027].
- [2] G. L. Kane, C. F. Kolda, L. Roszkowski and J. D. Wells, Phys. Rev. D **49** (1994) 6173 [arXiv:hep-ph/9312272]; J. R. Ellis, T. Falk, K. A. Olive and M. Schmitt, Phys. Lett. B **388** (1996) 97 [arXiv:hep-ph/9607292]; Phys. Lett. B **413** (1997) 355 [arXiv:hep-ph/9705444]; J. R. Ellis, T. Falk, G. Ganis, K. A. Olive and M. Schmitt, Phys. Rev. D **58** (1998) 095002 [arXiv:hep-ph/9801445]; V. D. Barger and C. Kao, Phys. Rev. D **57** (1998) 3131 [arXiv:hep-ph/9704403]; J. R. Ellis, T. Falk, G. Ganis and K. A. Olive, Phys. Rev. D **62** (2000) 075010 [arXiv:hep-ph/0004169].
- [3] J. R. Ellis, T. Falk, G. Ganis, K. A. Olive and M. Srednicki, Phys. Lett. B **510** (2001) 236 [arXiv:hep-ph/0102098].
- [4] V. D. Barger and C. Kao, Phys. Lett. B **518** (2001) 117 [arXiv:hep-ph/0106189]; L. Roszkowski, R. Ruiz de Austri and T. Nihei, JHEP **0108** (2001) 024 [arXiv:hep-ph/0106334]; A. Djouadi, M. Drees and J. L. Kneur, JHEP **0108** (2001) 055 [arXiv:hep-ph/0107316]; U. Chattopadhyay, A. Corsetti and P. Nath, Phys. Rev. D **66** (2002) 035003 [arXiv:hep-ph/0201001]; J. R. Ellis, K. A. Olive and Y. Santoso, New Jour. Phys. **4** (2002) 32 [arXiv:hep-ph/0202110]; H. Baer, C. Balazs, A. Belyaev, J. K. Mizukoshi, X. Tata and Y. Wang, JHEP **0207** (2002) 050 [arXiv:hep-ph/0205325]; R. Arnowitt and B. Dutta, arXiv:hep-ph/0211417.

- [5] J. R. Ellis, K. A. Olive, Y. Santoso and V. C. Spanos, *Phys. Lett. B* **565** (2003) 176 [arXiv:hep-ph/0303043]; H. Baer and C. Balazs, *JCAP* **0305**, 006 (2003) [arXiv:hep-ph/0303114]; A. B. Lahanas and D. V. Nanopoulos, *Phys. Lett. B* **568**, 55 (2003) [arXiv:hep-ph/0303130]; U. Chattopadhyay, A. Corsetti and P. Nath, *Phys. Rev. D* **68**, 035005 (2003) [arXiv:hep-ph/0303201]; C. Munoz, *Int. J. Mod. Phys. A* **19**, 3093 (2004) [arXiv:hep-ph/0309346]; R. Arnowitt, B. Dutta and B. Hu, arXiv:hep-ph/0310103; J. Ellis and K. A. Olive, In \*Bertone, G. (ed.): Particle dark matter\* 142-163 [arXiv:1001.3651 [astro-ph.CO]].
- [6] [The Muon g-2 Collaboration], *Phys. Rev. Lett.* **92** (2004) 161802, hep-ex/0401008; G. Bennett et al. [The Muon g-2 Collaboration], *Phys. Rev. D* **73** (2006) 072003 [arXiv:hep-ex/0602035].
- [7] ATLAS Collaboration, <https://cdsweb.cern.ch/record/1432199/files/ATLAS-CONF-2012-033.pdf>; S. Chatrchyan *et al.* [CMS Collaboration], *JHEP* **1210**, 018 (2012) [arXiv:1207.1798 [hep-ex]]; arXiv:1207.1898 [hep-ex].
- [8] G. Aad *et al.* [ATLAS Collaboration], *Phys. Lett. B* **716**, 1 (2012) [arXiv:1207.7214 [hep-ex]]; S. Chatrchyan *et al.* [CMS Collaboration], *Phys. Lett. B* **716**, 30 (2012) [arXiv:1207.7235 [hep-ex]].
- [9] G. Degrossi, S. Heinemeyer, W. Hollik, P. Slavich and G. Weiglein, *Eur. Phys. J. C* **28** (2003) 133 [arXiv:hep-ph/0212020]; S. Heinemeyer, W. Hollik and G. Weiglein, *Eur. Phys. J. C* **9** (1999) 343 [arXiv:hep-ph/9812472]; S. Heinemeyer, W. Hollik and G. Weiglein, *Comput. Phys. Commun.* **124** (2000) 76 [arXiv:hep-ph/9812320]; M. Frank *et al.*, *JHEP* **0702** (2007) 047 [arXiv:hep-ph/0611326]; See <http://www.feynhiggs.de>.
- [10] O. Buchmueller, *et al.*, arXiv:1207.7315 [hep-ph].
- [11] C. Stenge, G. Bertone, D. G. Cerdeno, M. Fornasa, R. R. de Austri and R. Trotta, *JCAP* **1203** (2012) 030 [arXiv:1112.4192 [hep-ph]]; P. Bechtle, T. Bringmann, K. Desch, H. Dreiner, M. Hamer, C. Hensel, M. Kramer and N. Nguyen *et al.*, *JHEP* **1206**, 098 (2012) [arXiv:1204.4199 [hep-ph]]; A. Fowlie, M. Kazana, K. Kowalska, S. Munir, L. Roszkowski, E. M. Sessolo, S. Trojanowski and Y. -L. S. Tsai, arXiv:1206.0264 [hep-ph]; T. Li, J. A. Maxin, D. V. Nanopoulos and J. W. Walker, arXiv:1206.2633 [hep-ph] and references therein.
- [12] O. Buchmueller, *et al.*, *Eur. Phys. J. C* **72** (2012) 2020 [arXiv:1112.3564 [hep-ph]].
- [13] H. Baer, V. Barger and A. Mustafayev, *Phys. Rev. D* **85**, 075010 (2012) [arXiv:1112.3017 [hep-ph]]; J. L. Feng, K. T. Matchev and D. Sanford, *Phys. Rev. D* **85**, 075007 (2012) [arXiv:1112.3021 [hep-ph]]; T. Li, J. A. Maxin, D. V. Nanopoulos and J. W. Walker, *Phys. Lett. B* **710** (2012) 207 [arXiv:1112.3024 [hep-ph]]; S. Heinemeyer, O. Stal and G. Weiglein, *Phys. Lett. B* **710**, 201 (2012) [arXiv:1112.3026 [hep-ph]]; A. Arbey, M. Battaglia, A. Djouadi, F. Mahmoudi and J. Quevillon, *Phys. Lett. B* **708**



- (2012) 162 [arXiv:1112.3028 [hep-ph]]; P. Draper, P. Meade, M. Reece and D. Shih, Phys. Rev. D **85**, 095007 (2012) [arXiv:1112.3068 [hep-ph]]; S. Akula, B. Altunkaynak, D. Feldman, P. Nath and G. Peim, Phys. Rev. D **85** (2012) 075001 [arXiv:1112.3645 [hep-ph]]; M. Kadastik, K. Kannike, A. Racioppi and M. Raidal, JHEP **1205** (2012) 061 [arXiv:1112.3647 [hep-ph]]; J. Cao, Z. Heng, D. Li and J. M. Yang, Phys. Lett. B **710** (2012) 665 [arXiv:1112.4391 [hep-ph]]; L. Aparicio, D. G. Cerdeno and L. E. Ibanez, JHEP **1204**, 126 (2012) [arXiv:1202.0822 [hep-ph]]; H. Baer, V. Barger and A. Mustafayev, JHEP **1205** (2012) 091 [arXiv:1202.4038 [hep-ph]]; C. Balazs, A. Buckley, D. Carter, B. Farmer and M. White, arXiv:1205.1568 [hep-ph]; D. Ghosh, M. Guchait, S. Raychaudhuri and D. Sengupta, Phys. Rev. D **86**, 055007 (2012) [arXiv:1205.2283 [hep-ph]].
- [14] J. Ellis and K. A. Olive, Eur. Phys. J. C **72**, 2005 (2012) [arXiv:1202.3262 [hep-ph]].
- [15] G. Aad *et al.* [ATLAS Collaboration], Phys. Lett. B **713**, 387 (2012) [arXiv:1204.0735 [hep-ex]]; T. Aaltonen *et al.* [CDF Collaboration], Phys. Rev. Lett. **107**, 239903 (2011) [Phys. Rev. Lett. **107**, 191801 (2011)] [arXiv:1107.2304 [hep-ex]]; updated results presented at Aspen in Feb. 2012 by M. Rescigno, <https://indico.cern.ch/getFile.py/access?contribId=28&sessionId=7&resId=1&materialId=slides&confId=143360>.; S. Chatrchyan *et al.* [CMS Collaboration], Phys. Rev. Lett. **107**, 191802 (2011) [arXiv:1107.5834 [hep-ex]]; R. Aaij *et al.* [LHCb Collaboration], Phys. Lett. B **699** (2011) 330 [arXiv:1103.2465 [hep-ex]]; arXiv:1203.4493 [hep-ex]; For an official combination of the ATLAS, CMS and LHCb results, see: ATLAS, CMS, and LHCb Collaborations, <http://cdsweb.cern.ch/record/1452186/files/LHCb-CONF-2012-017.pdf>.
- [16] R. Aaij *et al.* [LHCb Collaboration], arXiv:1211.2674 [Unknown].
- [17] H. Baer, A. Mustafayev, S. Profumo, A. Belyaev and X. Tata, Phys. Rev. D **71**, 095008 (2005) [arXiv:hep-ph/0412059]; H. Baer, A. Mustafayev, S. Profumo, A. Belyaev and X. Tata, JHEP **0507** (2005) 065, hep-ph/0504001.
- [18] J. R. Ellis, K. A. Olive and P. Sandick, Phys. Rev. D **78**, 075012 (2008) [arXiv:0805.2343 [hep-ph]].
- [19] D. Matalliotakis and H. P. Nilles, Nucl. Phys. B **435** (1995) 115 [arXiv:hep-ph/9407251]; M. Olechowski and S. Pokorski, Phys. Lett. B **344**, 201 (1995) [arXiv:hep-ph/9407404]; V. Berezhinsky, A. Bottino, J. Ellis, N. Fornengo, G. Mignola and S. Scopel, *Astropart. Phys.* **5** (1996) 1, hep-ph/9508249; M. Drees, M. Nojiri, D. Roy and Y. Yamada, *Phys. Rev. D* **56** (1997) 276, [Erratum-ibid. **D 64** (1997) 039901], hep-ph/9701219; M. Drees, Y. Kim, M. Nojiri, D. Toya, K. Hasuko and T. Kobayashi, *Phys. Rev. D* **63** (2001) 035008, hep-ph/0007202; P. Nath and R. Arnowitt, *Phys. Rev. D* **56** (1997) 2820, hep-ph/9701301; J. R. Ellis, T. Falk, G. Ganis, K. A. Olive and M. Schmitt, Phys. Rev. D **58** (1998) 095002 [arXiv:hep-ph/9801445]; J. R. Ellis, T. Falk, G. Ganis and K. A. Olive,

- Phys. Rev. D **62** (2000) 075010 [arXiv:hep-ph/0004169]; A. Bottino, F. Donato, N. Fornengo and S. Scopel, *Phys. Rev. D* **63** (2001) 125003, hep-ph/0010203; S. Profumo, *Phys. Rev. D* **68** (2003) 015006, hep-ph/0304071; D. Cerdeno and C. Munoz, *JHEP* **0410** (2004) 015, hep-ph/0405057.
- [20] J. Ellis, K. Olive and Y. Santoso, *Phys. Lett. B* **539**, 107 (2002) [arXiv:hep-ph/0204192]; J. R. Ellis, T. Falk, K. A. Olive and Y. Santoso, *Nucl. Phys. B* **652**, 259 (2003) [arXiv:hep-ph/0210205].
- [21] J. R. Ellis, K. A. Olive and P. Sandick, *Phys. Lett. B* **642**, 389 (2006) [hep-ph/0607002]; J. R. Ellis, K. A. Olive and P. Sandick, *JHEP* **0706**, 079 (2007) [arXiv:0704.3446 [hep-ph]]; J. R. Ellis, K. A. Olive and P. Sandick, *JHEP* **0808**, 013 (2008) [arXiv:0801.1651 [hep-ph]].
- [22] E. Cremmer, B. Julia, J. Scherk, P. van Nieuwenhuizen, S. Ferrara and L. Girardello, *Phys. Lett. B* **79**, 231 (1978); E. Cremmer, B. Julia, J. Scherk, S. Ferrara, L. Girardello and P. van Nieuwenhuizen, *Nucl. Phys. B* **147**, 105 (1979); For reviews, see: H. P. Nilles, *Phys. Rep.* **110** (1984) 1; A. Brignole, L. E. Ibanez and C. Munoz, arXiv:hep-ph/9707209, published in *Perspectives on supersymmetry*, ed. G. L. Kane, pp. 125-148.
- [23] A. H. Chamseddine, R. L. Arnowitt and P. Nath, *Phys. Rev. Lett.* **49**, 970 (1982); R. L. Arnowitt, A. H. Chamseddine and P. Nath, *Phys. Rev. Lett.* **50**, 232 (1983); R. Arnowitt, A. H. Chamseddine and P. Nath, arXiv:1206.3175 [physics.hist-ph].
- [24] R. Barbieri, S. Ferrara and C. A. Savoy, *Phys. Lett. B* **119**, 343 (1982).
- [25] J. Polonyi, Budapest preprint KFKI-1977-93 (1977).
- [26] V. D. Barger, M. S. Berger and P. Ohmann, *Phys. Rev. D* **49** (1994) 4908 [arXiv:hep-ph/9311269]; W. de Boer, R. Ehret and D. I. Kazakov, *Z. Phys. C* **67** (1995) 647 [arXiv:hep-ph/9405342]; M. Carena, J. R. Ellis, A. Pilaftsis and C. E. Wagner, *Nucl. Phys. B* **625** (2002) 345 [arXiv:hep-ph/0111245].
- [27] E. Dudas, Y. Mambrini, A. Mustafayev and K. A. Olive, arXiv:1205.5988 [hep-ph].
- [28] G. F. Giudice and A. Masiero, *Phys. Lett. B* **206**, 480 (1988).
- [29] L. Calibbi, Y. Mambrini and S. K. Vempati, *JHEP* **0709**, 081 (2007) [arXiv:0704.3518 [hep-ph]]; L. Calibbi, A. Faccia, A. Masiero and S. K. Vempati, *Phys. Rev. D* **74**, 116002 (2006) [arXiv:hep-ph/0605139]; E. Carquin, J. Ellis, M. E. Gomez, S. Lola and J. Rodriguez-Quintero, *JHEP* **0905** (2009) 026 [arXiv:0812.4243 [hep-ph]]; J. Ellis, A. Mustafayev and K. A. Olive, *Eur. Phys. J. C* **69**, 201 (2010) [arXiv:1003.3677 [hep-ph]]; J. Ellis, A. Mustafayev and K. A. Olive, *Eur. Phys. J. C* **69**, 219 (2010) [arXiv:1004.5399 [hep-ph]]; J. Ellis, A. Mustafayev and K. A. Olive, *Eur. Phys. J. C* **71**, 1689 (2011) [arXiv:1103.5140 [hep-ph]].

- [30] E. Dudas, A. Linde, Y. Mambrini, A. Mustafayev and K. A. Olive, arXiv:1209.0499 [hep-ph].
- [31] K. Choi, A. Falkowski, H. P. Nilles and M. Olechowski, Nucl. Phys. B **718** (2005) 113 [arXiv:hep-th/0503216]; K. Choi, K. S. Jeong and K. i. Okumura, JHEP **0509** (2005) 039 [arXiv:hep-ph/0504037]; M. Endo, M. Yamaguchi and K. Yoshioka, Phys. Rev. D **72** (2005) 015004 [arXiv:hep-ph/0504036]; A. Falkowski, O. Lebedev and Y. Mambrini, JHEP **0511** (2005) 034 [arXiv:hep-ph/0507110]; R. Kitano and Y. Nomura, Phys. Lett. B **631** (2005) 58 [arXiv:hep-ph/0509039]; R. Kitano and Y. Nomura, Phys. Rev. D **73** (2006) 095004 [arXiv:hep-ph/0602096]; A. Pierce and J. Thaler, JHEP **0609** (2006) 017 [arXiv:hep-ph/0604192]; K. Kawagoe and M. M. Nojiri, Phys. Rev. D **74**, 115011 (2006) [arXiv:hep-ph/0606104]; H. Baer, E.-K. Park, X. Tata and T. T. Wang, JHEP **0608** (2006) 041 [arXiv:hep-ph/0604253]; K. Choi, K. Y. Lee, Y. Shimizu, Y. G. Kim and K. i. Okumura, JCAP **0612** (2006) 017 [arXiv:hep-ph/0609132]; O. Lebedev, V. Lowen, Y. Mambrini, H. P. Nilles and M. Ratz, JHEP **0702** (2007) 063 [arXiv:hep-ph/0612035].
- [32] E. Komatsu *et al.* [WMAP Collaboration], Astrophys. J. Suppl. **192** (2011) 18 [arXiv:1001.4538 [astro-ph.CO]].
- [33] H. Goldberg, Phys. Rev. Lett. **50** (1983) 1419; J. Ellis, J. Hagelin, D. Nanopoulos, K. Olive and M. Srednicki, Nucl. Phys. B **238** (1984) 453.
- [34] E. Aprile *et al.* [XENON100 Collaboration], Phys. Rev. Lett. **107** (2011) 131302 [arXiv:1104.2549 [astro-ph.CO]].
- [35] S. Chen *et al.* [CLEO Collaboration], Phys. Rev. Lett. **87** (2001) 251807 [arXiv:hep-ex/0108032]; P. Koppenburg *et al.* [Belle Collaboration], Phys. Rev. Lett. **93** (2004) 061803 [arXiv:hep-ex/0403004]; B. Aubert *et al.* [BaBar Collaboration], arXiv:hep-ex/0207076; E. Barberio *et al.* [Heavy Flavor Averaging Group (HFAG)], arXiv:hep-ex/0603003.
- [36] ATLAS Collaboration,  
<https://cdsweb.cern.ch/record/1472710/files/ATLAS-CONF-2012-109.pdf>.
- [37] G. Abbiendi *et al.* [ OPAL Collaboration ], Eur. Phys. J. **C35**, 1-20 (2004) [hep-ex/0401026].
- [38] Information about this code is available from K. A. Olive: it contains important contributions from T. Falk, A. Ferstl, F. Luo, G. Ganis, A. Mustafayev, J. McDonald, K. A. Olive, P. Sandick, Y. Santoso, V. Spanos, and M. Srednicki.
- [39] M. Citron, J. Ellis, F. Luo, J. Marrouche, K. A. Olive and K. J. de Vries, arXiv:1212.2886 [hep-ph].
- [40] J. R. Ellis, K. A. Olive, Y. Santoso and V. C. Spanos, Phys. Lett. B **573** (2003) 162 [arXiv:hep-ph/0305212], and Phys. Rev. D **70** (2004) 055005 [arXiv:hep-ph/0405110].

- [41] O. Buchmueller, *et al.*, Eur. Phys. J. C **71**, 1583 (2011) [arXiv:1011.6118 [hep-ph]]; O. Buchmueller, *et al.*, Eur. Phys. J. C **71**, 1634 (2011) [arXiv:1102.4585 [hep-ph]]; O. Buchmueller, *et al.*, Eur. Phys. J. C **71**, 1722 (2011) [arXiv:1106.2529 [hep-ph]].
- [42] S. P. Martin, Phys. Rev. D **75**, 115005 (2007) [hep-ph/0703097 [HEP-PH]]; S. P. Martin, Phys. Rev. D **78**, 055019 (2008) [arXiv:0807.2820 [hep-ph]]; T. J. LeCompte and S. P. Martin, Phys. Rev. D **84**, 015004 (2011) [arXiv:1105.4304 [hep-ph]]; T. J. LeCompte and S. P. Martin, Phys. Rev. D **85**, 035023 (2012) [arXiv:1111.6897 [hep-ph]].